HELSINGIN YLIOPISTO
HELSINGFORS UNIVERSITET
UNIVERSITY OF HELSINKI

Master's Thesis
Department of Geosciences and Geography

Diatoms as a sea-ice proxy – improving the accuracy of sea-ice reconstruction by re-analysing the northern North Atlantic training set for *Fragilariopsis oceanica, Fragilariopsis reginae-jahniae* and *Fossula arctica*, in addition to the chrysophyte cyst *Archaeomonas* sp.

7th May 2019

Benjamin Heikki Redmond Roche

Faculty of Science
P.O. Box 64 (Gustaf Hällströmin Katu 2)
FI-00014 University of Helsinki, Finland

Abstract

Faculty: Faculty of Science	Department: Geology – Palaeontology and Global Change	
Author: Benjamin Heikki Redmond Roche		
Title: Diatoms as a sea-ice proxy – improving the accuracy of sea-ice reconstruction by re-analysing the northern North Atlantic training set for *Fragilariopsis oceanica, Fragilariopsis reginae-jahniae* and *Fossula arctica*, in addition to the chrysophyte cyst *Archaeomonas* sp.		
Subject: Micropalaeontology/Palaeoceanography/Geology		
Level: Master's Thesis	Month and year: 7.05.19	Number of pages: 70

Abstract: (34 lines – Size 10: Arial)

Significant changes in sea-ice variability have occurred in the northern North Atlantic since the last deglaciation, resulting in global scale shifts in climate. By inferring the dynamic changes of palaeo sea-ice to past changes in climate, it is possible to predict future changes in response to anthropogenic climate change. Diatoms allow for detailed reconstructions of palaeoceanographic and sea-ice conditions, both qualitatively, using information of species ecologies and quantitatively, via a transfer function based upon diatom species optima and tolerances of the variable to be reconstructed. Three diatom species comprising a large portion of the training set are proxies for the presence of sea ice: *Fragilariopsis oceanica, Fragilariopsis reginae-jahniae* and *Fossula arctica*, have currently been grouped into one species – *F. oceanica* – in the large diatom training set of the northern North Atlantic region. The clustering of the species may result in an imprecise reconstruction of sea ice that does not take into account all the available ecological information.

The proportions of the three species were recounted from the original surface sediment slides alongside the additional chrysophyte cyst *Archaeomonas* sp. and statistically analysed using Canoco and the R software package eHOF. A core from Kangerlussuaq Trough comprising the Late Holocene (~690–1498 Common Era) was also recounted and analysed using C2.

The separated diatom species and chrysophyte cyst *Archaeomonas* sp. exhibited different relationships to both sea-ice concentration (aSIC) and sea surface temperature (aSST). The separated *F. oceanica* is a 'cold-mixed' water species occurring at cold aSST and both low and high aSIC. High abundances occur in the marginal ice zone (MIZ) where surficial meltwater is high during the spring bloom, with additional inputs from glacial meltwaters nearshore. *F. reginae-jahniae* is a sea-ice associated species related to cold aSST and high aSIC. High abundances occur in the low salinity Arctic Water dominated MIZ which experiences significant aSIC. *F. arctica* is a sea-ice associated species related to cold aSST and high aSIC. High abundances occur in the low salinity Arctic Water dominated MIZ which experiences high aSIC, particularly in polynya conditions. *F. arctica* can be considered a characteristic polynya species at high abundances. *Archaeomonas* sp. is a 'cold-mixed' water species related to both cold and relatively warm aSST and low and high aSIC. High abundances occur in both relatively warm ice-free Atlantic Water and also in cold high aSIC Arctic Water conditions rendering it a more complex indicator for aSST or aSIC proxy. However, the aversion to MIZ conditions indicates that *Archaeomonas* sp. is associated with a relatively saline unstratified water column. This is the first time that the distribution and ecology of *Archaeomonas* sp. has been presented. As such, the ecology described here can be used in future studies. The separation of the three diatom species is crucial for the ecological interpretation of downcore assemblage changes. It is also crucial for the application of transfer functions in order to have greater precision in reconstructing aSIC and assessing the influence of Arctic Water or Atlantic Water, even at low abundances.

Keywords:
Diatoms, sea ice, North Atlantic, *Fragilariopsis oceanica*, *Fragilariopsis reginae-jahniae*, *Fossula arctica*, chrysophyte cyst *Archaeomonas* sp., species ecology, transfer function, redundancy analysis, Arctic Water, Atlantic Water.

Where deposited:
HELDA – Digital Repository of the University of Helsinki

Additional information:
Submitted to the thesis committee before the deadline of 17.5.19, for grading at the board meeting on 24.5.19.

Table of Contents

1. INTRODUCTION

1.1. Sea ice and the climate system

Arctic Sea-ice extent is considered to be an area of ocean with at least 15% sea ice present, measured using radiometry data and visible imagery collected from Polar orbiting satellites. The 1981–2010 median range of Arctic Sea-ice extent varies from a maximum of 15.5 million km^2 in March to a minimum of 6.3 million km^2 in September (NSIDC, www.nsidc.com). In 2018 this decreased to 14.3 million km^2 in March and 4.7 million km^2 in September (Fetterer *et al*. 2018). Multiyear sea-ice occurs in the Arctic Ocean northwards of 78°N to the west of Greenland and 81°N to the east of Greenland, whilst seasonal sea-ice stretches to 59°N to the west and 75°N to the east, primarily due to the effect of the Gulf Stream (Tang *et al*. 2004; Fetterer *et al*. 2018). The marginal ice zone (hereinafter referred to as MIZ) is a part of the seasonal ice pack that is affected by open ocean, either from currents or the physical effect of waves, resulting in various forms of sea-ice types or forms such as new ice, nilas or pancake ice (Wadhams, 2000).

Large-scale variability in Arctic sea-ice content has an impact on global climate through changes to the energy balance of the Earth and to atmospheric and oceanic circulation (Budikova, 2009). Variations in orbital cycles result in amplified changes upon the poles, which in turn have inherently regulated the transitions between stadial and interstadial periods since glaciation began in the Quaternary Period (Ehlers, 2011). The albedo difference between sea ice (~0.5–0.7) and seawater (~0.06) results in vast changes in the amount of incoming solar radiation the Earth receives (Curry & Schramm, 1995). A large decrease in the albedo of the North Pole can lead to positive feedbacks affecting the climate and ecosystems of the entire planet, particularly when coupled with the increase in anthropogenically-sourced CO_2 emissions. This is particularly significant as a dramatic decrease in Arctic sea-ice extent could lead to runaway warming if CO_2 continues to increase alongside decreasing albedo; as Shakun *et al*. (2012) established that during the last deglaciation only 7% of global temperature increase was caused by orbital forcing, whereas 93% occurred in response to increasing CO_2. Thus, decreasing polar sea-ice is the fundamental precursor to dramatically enhanced warming caused by an increased greenhouse effect. Furthermore, increasing greenhouse gas inputs are expected to have the most significant effect upon Arctic climate

than anywhere else (Kattsov *et al*. 2005). Mean global temperatures are projected to rise by 2.5°C and 3.5°C by 2100, based upon greenhouse emissions scenarios B2 and A2 respectively, proposed by the Intergovernmental Panel on Climate Change (IPCC, 2001; AMAP, 2017). Over the same period, Arctic temperatures according to scenarios B2 and A2 are predicted to rise by 5°C and 7°C respectively, according to models derived from the Arctic Climate Impact Assessment, epitomising the magnified polar warming associated with climate change (IPCC, 2001; Kattsov *et al*. 2005; AMAP, 2017).

1.2. Reconstructing past sea ice

Palaeoclimate reconstructions are fundamental for providing a base from which future trajectories can be projected and assessed. By studying past decadal-to-millennial scale climate variability and better understanding the mechanisms behind both natural and anthropogenic forcing, it is possible to model future climate change (Miettinen, 2018). Geological proxies such as diatom and dinoflagellate cyst assemblages, biomarkers, foraminiferal $\delta^{18}O$ and ice-rafted debris – are used to reconstruct palaeoclimatic conditions (Calvert & Pedersen, 2007). The strength of the knowledge of the applied proxies is fundamental to the accuracy of the reconstruction. Biogenic sea-ice proxies have a regional significance due to the differing bioeconoses developed by boreal and austral species in the Arctic since the Cenozoic (de Vernal *et al*. 2013). Complementary application of the sea-ice proxies suggested in de Vernal *et al*. (2013) (diatoms, dinoflagellate cysts, ostracods, foraminifers, IP_{25}, highly branched isoprenoids, methanesulfonic acid in ice and sea salt in ice) would give the most comprehensive sea ice reconstructions.

1.3. Diatoms as sea-ice proxies

Marine diatoms constitute ~40% of the total primary production in modern oceans and over 50% of organic carbon burial in marine sediments (Tréguer *et al*. 1995; Falkowksi *et al*. 2004; Jordan & Stickley, 2010). They are siliceous unicellular phytoplankton which inhabit the uppermost ~50 metres of the epipelagic zone, blooming in spring and summer when high latitude sunlight is sufficient, and the greatest quantity of sea-ice melting occurs (ji *et al*. 2013; Leu *et al*. 2015). Some species are sympagic rather than planktic and physically inhabit the ice

(Brown & Belt, 2017). They are regarded as one of the principal palaeoclimatic proxies for reconstructing sea surface temperature, the sea-ice margin and the distribution of water masses (Koç & Schrader, 1990; Andersen *et al*. 2004a). As such, substantial qualitative and quantitative diatom-based study has been undertaken for the Quaternary and Holocene in the northern North Atlantic (e.g. Williams, 1986; 1990; 1993; Koç Karpuz & Schrader, 1990; Koç & Jansen, 1994; De Sève, 1999; Jiang *et al*. 2001; 2002; 2005; 2015; Koç *et al*. 2002; Andersen *et al*. 2004a; 2004b; Witak *et al*. 2005; Berner *et al*. 2008; Justwan & Koç, 2008; 2009; Justwan *et al*. 2008; Ren *et al*. 2009; Krawczyk *et al*. 2010; 2013; 2014; 2016; Miettinen *et al*. 2011; 2012; 2015; Weckström *et al*. 2013; Pearce *et al*. 2014a; 2014b; Xiao *et al*. 2017; Oksman *et al*. 2017a; 2017b; 2019;), and can potentially be applied as far back as the Early Cretaceous (Gersonde & Harwood, 1990).

In modern high-latitude polar seas, marine diatoms are very diverse and abundant, exhibiting strong relationships to sea surface hydrographic environments such as temperature and varying sea-ice conditions (Koç & Schrader, 1990; Andersen *et al*. 2004a; Miettinen *et al*. 2012; Oksman *et al*. 2019). Diatoms from surface sediments (top 1 cm) are representative of the overlying sea-surface conditions, thus the ecology of diatoms analysed from surface sediment can be applied as an analogue for palaeo sea surface conditions (Jordan & Stickley, 2010). By understanding the ecology and current geographical range of extant diatoms, it allows for their use as indicator species in qualitative and quantitative reconstructions (Oksman *et al*. 2019). Downcore palaeoceanographic and palaeoclimatic conditions can then be inferred from the relative abundances of the indicator species present (Andersen *et al*. 2004b; Krawczyck *et al*. 2016; Oksman *et al*. 2019). Of particular significance to this study is the presence of sea-ice indicator diatom species as they allow for robust reconstructions of past sea-ice variability (Berner *et al*. 2008).

Diatoms are an important information source of Arctic sea-ice variability during the Holocene – be it from the relative abundance of sea-ice indicator species or changing fluxes in the biomarker IP_{25} (Belt & Müller, 2013). IP_{25} (Ice proxy with 25 carbon atoms) is an alkene that is preserved in sediments; produced by some diatom species in the genera *Haslea* and *Pleurosigma,* which occupy the interstitial channels in the lowermost part of sea ice and thus, high fluxes of it are indicative of the presence of sea ice (Belt *et al*. 2007; Belt & Müller, 2013).

To quantitatively reconstruct past environmental conditions from diatoms, it is necessary to first establish a modern diatom-environment training set which applies modern surface-sediment biological data with contemporary environmental conditions (Juggins & Birks, 2012). It is then necessary to determine the relationship between modern environments (such as temperature and sea ice conditions) with the occurrences and abundances of diatom species in the training set to develop a model via various numerical techniques (Juggins & Birks, 2012). Once this model has been developed, it can be applied as a transfer function to infer palaeoclimatic and palaeoceanographic conditions. Therefore, the strength of this model is inherently derived from the quality of known ecologies for diatom species present in the training set and their preferred environmental conditions.

Three diatom species that are proxies for the presence of sea ice: *Fragilariopsis oceanica, Fragilariopsis reginae-jahniae* and *Fossula arctica*, have currently been grouped into one species in an extensive training set from the North Atlantic region under *F. oceanica* (Andersen *et al*. 2004a, 2004b; Miettinen *et al*. 2015; Oksman *et al*. 2019). The aim of this study is to re-analyse and separate the *F. oceanica* species complex in the training set used in Miettinen *et al*. (2015) into the three above described and microscopically distinguishable species. This will allow for a more detailed picture of the oceanography of the North Atlantic region – specifically with regards to sea-ice environments. The differences in ecology of the three taxa can be used as a tool to better understand their environment and to improve palaeoceanographic reconstructions – particularly changes in sea-ice variability. It is currently unclear if these species have a different response to the various sea ice conditions, thus better understanding of their ecologies will permit for more comprehensive analysis of sea-ice variability in the northern North Atlantic (Weckström, 2019, personal communication).

The three species resemble each other morphologically and consequently skilled microscopy is required to separate them. These species have previously been inferred to all simply represent the presence of sea ice and so, coupled with their resemblances, are grouped together under one species – as *F. oceanica* in the North Atlantic training set used in a large number of diatom-inferred sea surface temperature and sea ice reconstructions in the region (e.g. Miettinen *et al*. 2015; Krawczyk *et al*. 2016; Oksman *et al*. 2017a; 2017b). Further, *Fossula arctica* and *Fragilariopsis reginae-jahniae* were described as separate species

relatively lately (Hasle *et al*. 1996; Witkowski *et al*. 2000 - respectively), which is also a contributing factor as to why they are not included in the dataset as a significant part of the Miettinen *et al*. (2015) training set was collected and analysed in the 1990s.

Diatom analysis can lead to both quantitative and qualitative investigations of palaeoceanographic environments. However, the relatively unknown species-specific ecology is apparent through the discrepancies that different studies have in the interpretation of diatom ecologies. For instance, *Fragilariopsis cylindrus* is not regarded as a straightforward sea-ice indicator species in Oksman *et al*. (2019) but is in Ren *et al.* (2009). Similarly, *Fragilariopsis oceanica* is regarded as an 'open marine' diatom in Krawczyk *et al*. (2016) and is found to have a statistically significant relationship to sea-ice in Oksman *et al*. (2019), whilst von Quillfeldt (2000) ascribes it to large pulses of meltwater. This close proximity to meltwater (von Quillfeldt, 2000) allowed for the interpretation of surface warming and glacier retreat in central-eastern Baffin Bay during the Holocene (Oksman *et al*. 2017a); and equally, to the increased meltwater signal found in the southwestern Labrador Sea coincident with Greenland Ice Sheet minimum at the end of the Holocene Thermal Maximum (Weckström, 2019, Personal Communication). The relative abundance of *Fragilariopsis oceanica* was high in both instances and therefore without consideration of the relationship to meltwater, it would be easy to infer these abundances as indicative of increased sea ice (von Quillfeldt, 2000; Oksman *et al*. 2017a; Weckström, 2019, Personal Communication). Hence, more accurate interpretation of the ecologies of these sea-ice indicator diatoms is fundamental to clarifying our understanding of sea-ice variability.

The crysophyte cyst *Archaeomonas* sp. is a common species in cold waters associated with the MIZ off Antarctica, although little is known about it in the Arctic realm (Riaux-Gobin & Stumm, 2006). The *Archaeomonas* cysts are relatively common in core and surface sediment samples from the MIZ in the Arctic but are rarely included in counts (Weckström, 2019, Personal Communication). Thus, by also counting the abundances of this species in this work, it is possible to shine a light upon their ecology and indicate whether they are a potential sea-ice indicator species.

1.4. Quaternary climate and sea-ice variability

Northern Hemisphere Glaciation began gradually (~2.9–2.4 Ma) and resulted in the formation of the Greenland ice sheet: a fundamental regulator of Pleistocene glacial-interglacial climate (Raymo, 1994; Bartoli *et al*. 2005). The final closure of the Central American Seaway (~3–2.5 Ma) resulted in a stronger Atlantic thermohaline conveyor therefore enhancing the supply of moisture, salt and heat in the Gulf Stream (Bartoli *et al*. 2005). This low- to mid-latitude deep water warming enhanced Northern Hemisphere glaciation, in what is termed the 'snow gun hypothesis', resulting in the formation of the Greenland ice sheet (Prentice & Matthews, 1991; Bartoli *et al*. 2005). The glaciation resulted in an irreversible 'climate crash' (~2.74 Ma) during which Arctic sea-ice increased in response to cooling and freshwater build-up (Lisiecki & Raymo, 2005; Polyak *et al*. 2010). Decreased sea-ice conditions, with the Arctic Ocean having possibly been seasonally ice free, occurred during interglacials which had a periodicity of ~41 Ka in the Early to Mid-Quaternary (~2.6–1 Ma) and ~100 Ka in the Late Quaternary (~1–0.011 Ma) (Imbrie & Imbrie, 1986; Polyak *et al*. 2010).

Since the Last Glacial Maximum peak conditions ~22.1 Ka in the Northern Hemisphere and ~22.3 Ka in the Southern Hemisphere, global climate has steadily warmed and Arctic sea-ice has decreased, indicative of a coincident hemispheric warming (Shakun & Carlson, 2010). This coincident hemispheric warming is attributed to a combination of increased insolation, increased CO_2 and alterations to the thermohaline conveyor in the northern Atlantic (shakun & Carlson, 2010). The average global temperature was ~4.9°C colder during the Last Glacial Maximum, with a range of ~0.5°C cooler in the tropics, to ~17°C cooler in the Arctic (Shakun & Carlson, 2010). The magnitude of glacial-interglacial changes increased with latitude and are evidential for the polar amplification of climate change, particularly in the northern high latitudes (Shakun & Carlson, 2010). From the end of the Last Glacial Maximum global climate warmed relatively steadily until the Younger Dryas cold period (~12.9–11.7 Ka), where a ~2–8°C Northern Hemisphere cooling occurred north of 35°N, and a ~1–2°C warming occurred south of ~45°S (Shakun & Carlson, 2010; Carlson, 2013). This bipolar seesaw is attributed to a large meltwater influx into the northern North Atlantic primarily derived from the waning Laurentide Ice Sheet, lasting for ~1200 years, and resulting in the near shutdown of the Atlantic meridional overturning circulation (hereinafter referred to as AMOC) (Broecker,

2006; Carlson, 2013). Additional meltwater from the Scandinavian Ice Sheet into the Nordic Seas, a large influx of icebergs through the Hudson Strait and increased formation of North Atlantic sea-ice in response to fresher surface waters may have also contributed to the near shutdown of the AMOC (Seager *et al*. 2002; Broecker, 2006; Muschitiello, 2016).

The Holocene commenced as climate warmed at the end of the Younger Dryas (~11.65 Ka). Warming in the Nordic Seas and decreased sea ice is attributed to higher insolation and stronger fluxes of North Atlantic Drift in the north-eastern Atlantic (Andersen *et al*. 2004a). A transient cold period occurred (~8.4–8.0 Ka) as the final deglaciation of the Laurentide Ice Sheet, via the Hudson Strait, into the Labrador Sea disrupted the AMOC and caused an abrupt ~5°C cooling in the Northern Hemisphere (Alley *et al*. 1997; Kobashi *et al*. 2007; Hoffman *et al*. 2012). April sea-ice concentrations in Baffin Bay were depressed during the Holocene Climate Optimum (~7.5–3.5 Ka) coinciding with minimum extents of the Greenland Ice Sheet (Moros *et al*. 2016; Krawczyk *et al*. 2016). A cooler period followed with increased sea ice in both Baffin Bay and the Greenland Sea (Moros *et al*. 2016; Oksman *et al*. 2017b).

During the Roman Warm Period (~2.3–1.5 Ka) low sea-ice concentrations were prevalent to the west of Greenland, and surface waters became fresher from increased glacial meltwater (Seidenkrantz *et al*. 2008; Krawczyck *et al*. 2016). Subsurface waters experienced large influxes of Atlantic Water from a warmer or stronger West Greenland Current (Lloyd *et al*. 2007; Seidenkrantz *et al*. 2008). An antiphase climatic relationship developed to the west and east of Greenland during the Medieval Climate Anomaly (~1.2–0.7 Ka), when sea ice to the east of Greenland decreased coincidentally to increased sea ice west of Greenland and In the Labrador Sea (Seidenkrantz *et al*. 2008; Mann *et al*. 2009; Miettinen *et al*. 2015; Krawczyk *et al*. 2016). the increase in sea ice concentration, significantly cooler waters off Disko Bay and advance of the Jakobshavn Isbræ glacier, indicate a decreased influence of Atlantic Water (Seidenkrantz *et al*. 2008; Krawczyk *et al*. 2016). An inverse antiphase climate relationship developed to the west and east of Greenland during the Little Ice Age (~0.7–0.15 Ka) when decreased sea ice prevailed in the Labrador Sea, indicative of increased Atlantic Water input, concurrent to sea ice increasing east of Greenland (Seidenkrantz *et al*. 2007; Miettinen *et al*. 2015; Krawczyk *et al*. 2016). These northwest and northeast Atlantic antiphase relationships have been attributed to centennial scale variations in North Atlantic oscillation (hereinafter

referred to as NAO) – with a positive NAO during the Medieval Climate Anomaly and negative NAO during the Little Ice Age (Seidenkrantz *et al.* 2007; 2008; Krawczyck *et al*. 2013; 2016).

Since the end of the Little Ice Age, global climate has warmed intensely. The onset of the industrial revolution fundamentally altered humanity and our impact upon the planet. Changes have been so significant, particularly increases in CO_2 and CH_4, that Crutzen & Stoermer (2000) argued that we had now entered the Anthropocene Epoch: an identifiable horizon in the geological record, from greenhouse gases in ice cores to 'technofossils' and radionuclides preserved in stratigraphy (Waters *et al*. 2016). Since the glacial-interglacial cycle began in the Pleistocene Epoch, atmospheric CO_2 has fluctuated between 180–280 ppm. In 2013 the 400 ppm threshold was crossed for the first time since ~3 Ma, when temperatures were ~4°C warmer, sea levels were ~20 m higher than present and the Arctic Ocean may have been seasonally ice-free (Polyak *et al*. 2010; Monastersky, 2013; Haywood *et al*. 2016). In unison with this extremely rapid CO_2 increase is the exceptional warming that has occurred in the 20th and 21st century, dwarfing in magnitude the warming of the Medieval Climate Anomaly (Mann & Jones, 2003). Since pre-industrial times at the end of the Little Ice Age, human activity has caused ~1°C of warming, with temperature predicted to rise to ~1.5°C potentially as soon as 2030 (IPCC, 2018). In response to this warming September Arctic sea-ice extents are currently decreasing at 12.8% per decade relative to the 1981–2010 average (NSIDC, www.nsidc.com).

1.5. Aims of the thesis

The aim of this study is to improve the accuracy of specific sea ice indicator species by separating the diatom species *F. oceanica, F. reginae-jahniae* and *F. arctica* and additionally counting the chrysophyte cyst *Archaeomonas* sp. from the Miettinen *et al*. (2015) training set. The data counts will be quantitatively analysed in a refined training set to infer the relationship of the individual species to the environmental variable's sea ice concentration and sea surface temperature. The Core MD99-2322 from Miettinen *et al*. (2015) will be recounted for the Late Holocene to apply the new found ecological data either qualitatively or quantitatively. The main hypothesis is that the three diatom species will have individual relationships to varying sea ice conditions and therefore afford more robust

palaeoceanographic reconstructions through their separation. Secondly, that the relatively high abundance of the chrysophyte cyst *Archaeomonas* sp. in the northern North Atlantic may result in it potentially being a useful indicator species if it is associated with sea ice.

2. STUDY SITE

The training set encompasses 46 localities from the northern North Atlantic, between 74°5'31.43"N, 78°43'7.10"W in the West to 76°28'43.97"N, 14°35'17.12"E in the East; and 61°27'49.25"N, 58°2'9.02"W in the South to 78°33'42.34"N, 5°14'26.70"E in the North (Figure 1). The localities are evenly split with 23 to the west of Greenland in Baffin Bay and the Labrador Sea, and 23 to the east of Greenland in the Nordic Seas (Greenland, Norwegian and Baffin Seas). To the west of Greenland, maximum sea-ice extent reaches far southwards into the Labrador Sea, with Baffin and Hudson Bays mostly freezing (Wang *et al*. 1993). To the east of Greenland, maximum sea-ice extent is limited to the waters around Svalbard in the north and along the east Greenland margin (Serreze *et al*. 2003). This dichotomous sea-ice extent at parallel latitudes to the west and east of Greenland is fundamentally attributed to the transfer of heat by the Gulf Stream and the strength of NAO (Taylor & Stephens, 1998).

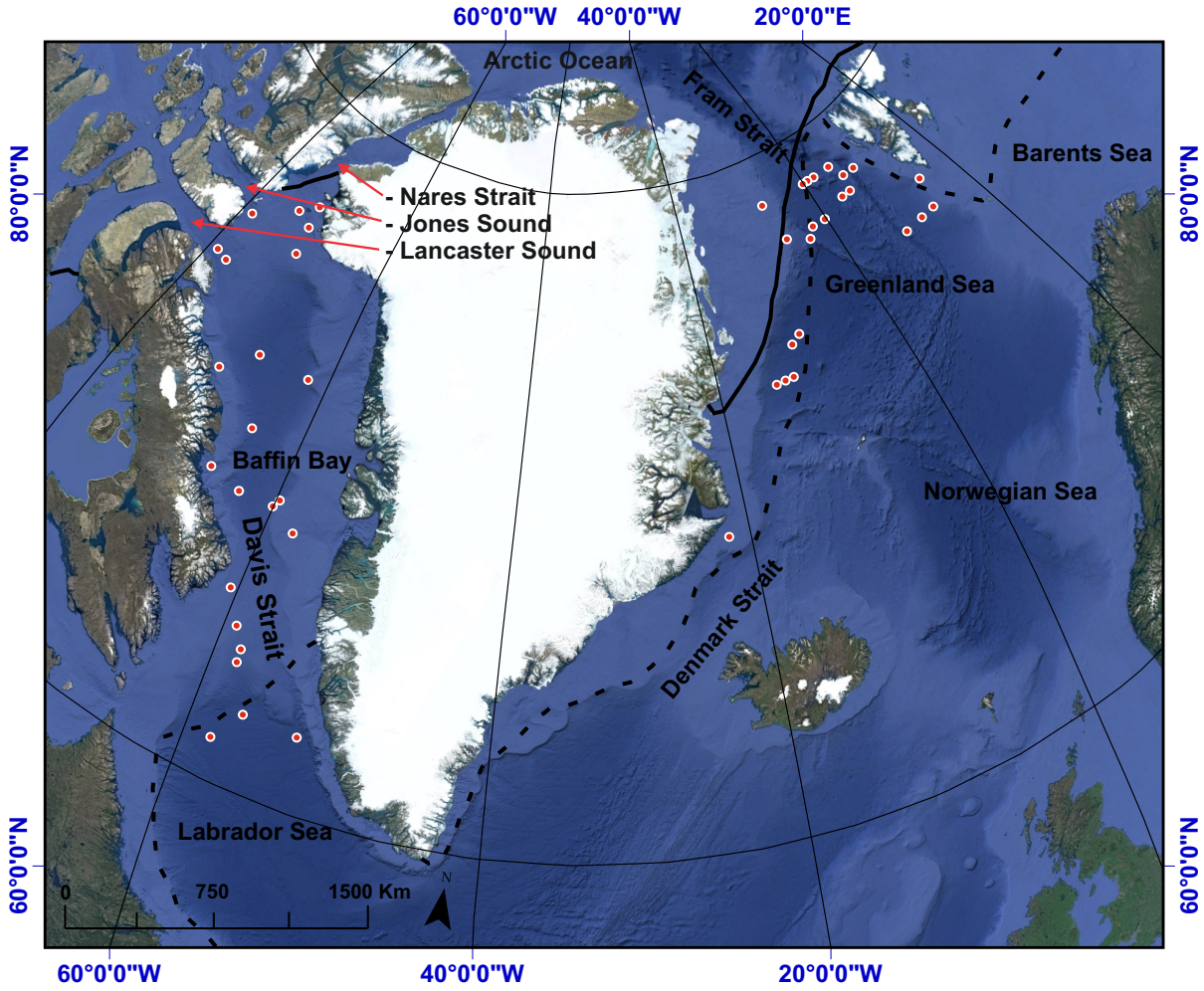

Figure 1: Projected coordinate system map of the northern North Atlantic, with data point localities superimposed. Dashed line**:** Winter sea-ice maximum (March), and continuous line**:** Summer sea-ice minimum (September) (Fetterer *et al*. 2018). Base map from Google Earth Pro.

2.1. Bathymetry

The northern North Atlantic Ocean around Greenland varies tremendously in both geology and depth, with the relatively enclosed Baffin Bay, Davis Strait and Canadian Arctic Archipelago to the west; and the large open Nordic Sea's and Svalbard, Jan Mayen and Iceland to the east.

Baffin Bay is a small marginal sea with an area of 1400 km by 550 km (689,000 km^2), connected to the Arctic Ocean via the Nares Strait, Jones and Lancaster Sounds to the north and the Labrador Sea via the Davis Strait to the south (Tang *et al*. 2004). Seafloor spreading separating Baffin Bay and Greenland occurred between ~62–61.7 Ma (magnetic chron 27) and ceased by ~34.8–33.3 Ma (magnetic chron 13) (Müller *et al*. 2008; Funck *et al*. 2012). In the Baffin Basin

there is a deep abyssal plain, exceeding 2300 m depth, which is flanked by a narrow continental shelf on the Baffin Island margin and a much thicker continental shelf on the Greenland margin, where depths remain above 500 m and terrigenous sediment deposition is high (Figure 2). The continental shelves are deeply scoured by cross cutting canyons which can exceed 800 m depth (Tang *et al*. 2004). The Davis Strait connects Baffin Bay and the Labrador Sea via a 170 km wide channel with a maximum sill depth of 650 m (Tang *et al*. 2004). The Kane Basin in the Nares Strait connects Baffin Bay to the Arctic Ocean between Ellesmere Island and Greenland via a 250 m deep sill. To the north, the channel width is restricted to less than 40 km in the Robeson Channel (Tang *et al*. 2004). The Jones Sound located between Devon Island and Ellesmere Island has a 120 m deep sill in its westernmost point at the 30 km wide Hells Gate (Tang *et al*. 2004). The Lancaster Sound located between Devon Island and Baffin Island has a 125 m deep sill through the 55 km wide Barrow Strait (Tang *et al*. 2004).

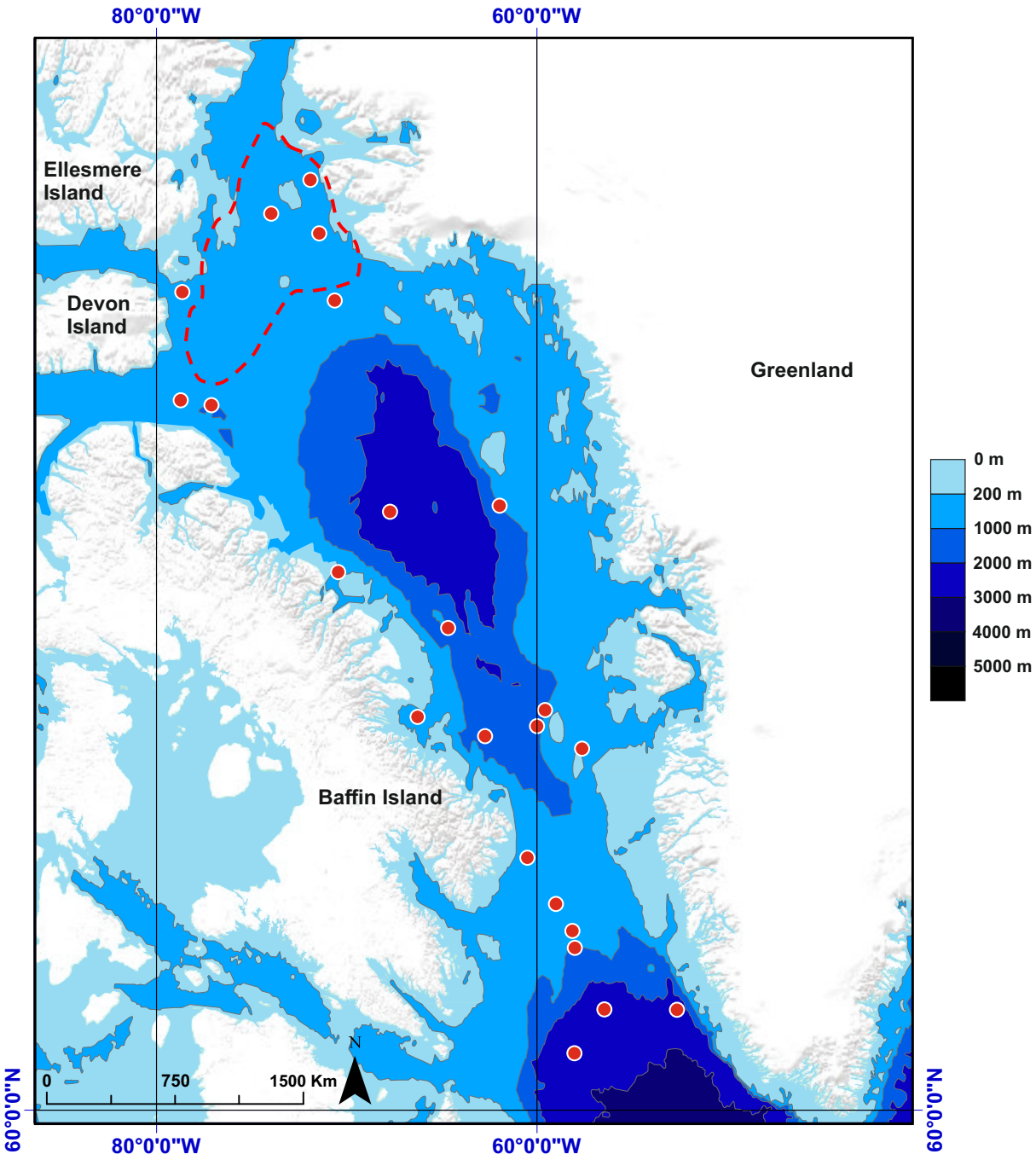

Figure 2: Geographic coordinate system bathymetric map west of Greenland: the northern Labrador Sea, Baffin Bay, Davis Strait, Nares Strait, Jones Sound and Lancaster Sound, with data point localities superimposed. Dashed red line indicating the average location of the North Water Polynya according to Christie & Sommerkorn (2012). Base Map from ESRI and bathymetric data from Natural Earth.

The Greenland Sea is a large expanse of open ocean covering 1,205,000 km^2, connected to the Arctic Ocean to the north via the Fram Strait; the Barents Sea to the east, Norwegian Sea to the southeast (combining to form the Nordic Seas) and Denmark Strait to the southwest (Vogt, 1986). The Greenland Sea is flanked to the west by Greenland, the Svalbard archipelago to the east and Jan Mayen and Iceland to the south. Ongoing seafloor spreading separating

Greenland from Norway began ~53 Ma (magnetic chron 24), along the Kolbeinsey, Mohns, Knipovich and Molloy Ridge's running south to north from Iceland (Vorren *et al*. 1998; Müller *et al*. 2008). Greenland and Svalbard separated 38 Ma (magnetic chron 13), concurrent to the opening of the Labrador Sea (Talwani & Eldholm, 1977). The East Greenland Continental Shelf has a depth ranging from less than 100 m to 300 m and varying in width from a minimum of 30 km in the south, to 280 km in the north, with high terrigenous sediment input (Figure 3) (Vorren *et al*. 1998). Along the southern margin of the shelf (~70°N), the slope drops from 400 m to 1600 m along a gradient of 1:38; along the northern margin of the shelf (~82°N), the slope drops from 400 m to 3400 m along a gradient of 1:13 (Vorren *et al*. 1998). The shelf is scoured with deep trenches exceeding 500 m, particularly Scoresby Sund, one of the largest and longest fjord systems in the world which in parts exceeds 1400 m depth (Migoń, 2010). The Greenland Sea exceeds 2000 m depth in the Icelandic Plateau between Iceland and Jan Mayen, where the Kolbeinsey Ridge trends NNE (Jakobsson *et al*. 2012). Northwards of the Jan Mayen Fracture Zone there is a significant increase in depth as the Greenland Abyssal Plain far exceeds 3000 m depth, with a maximum depth of 3606 m. The 2000 m deep southeast trending East Greenland Ridge separates the Greenland Abyssal Plain from the Boreas Abyssal Plain to the north, which also exceeds 3000 m depth (Jakobsson *et al*. 2012). The Fram Strait connects the Greenland Sea to the Arctic Ocean via a 300 km wide sill with a depth of 2545 m between the continental shelves (Soltwedel *et al*. 2003). A small basin within the Fram Strait, the Molloy Deep, has a maximum depth of 5607 m and is the deepest point in both the Fram Strait and Arctic Ocean (Soltwedel *et al*. 2003).

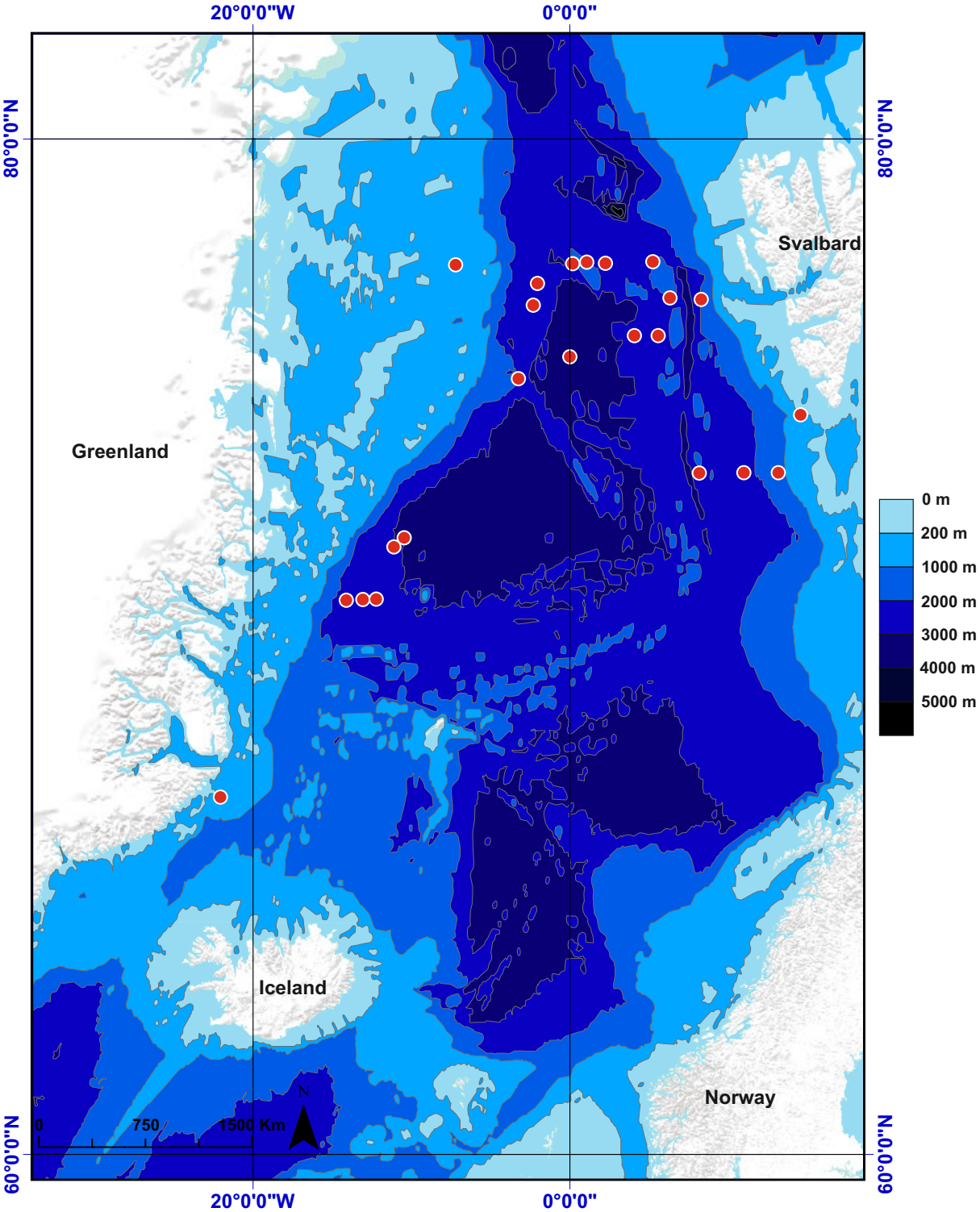

Figure 3: Geographic coordinate system map of east of Greenland: The Nordic Seas, Fram Strait and Denmark Strait, with data point localities superimposed. Base Map from ESRI and bathymetric data from Natural Earth.

The Barents Sea to the south of Svalbard has an average depth of less than 500 m (Jakobsson *et al*. 2012). It covers 1500 km of continental shelf, composed of ~7 km of Late Cenozoic clastic sediments (Vorren *et al*. 1998). The slope from the continental shelf to 2000 m depth to the

east of the Knipovich Ridge is much more gradual than it is from the East Greenland Shelf. The axial valleys of the mid ocean ridges tend to be at a depth exceeding 2500 m and constantly exceeding 3000 m further north along the Knipovich ridge. The Yermak Plateau stretching for 500 km northwards of Svalbard also has an average depth of less than 500 m, gradually sloping into the Arctic Ocean. The narrow Denmark Strait sill has a depth of 640 m, which extends for 480 km between southeast Greenland and Iceland and joins the Irminger Basin to the south (Mauritzen, 1996; Rudels *et al*. 2002). This Greenland-Iceland-Scotland Ridge is continued eastwards of Iceland, with the Iceland-Faeroe Ridge exceeding 500m depth, and the Faeroe-Shetland Ridge exceeding 800 m depth and separating the Iceland Basin to the south (Mauritzen, 1996).

2.2. Physical oceanography

The climate of the Earth is in part regulated and determined by the oceans, the variability of currents and their interactions with the land surface and atmosphere. Thermohaline circulation is the fundamental transport mechanism of heat from the tropics to the poles on Earth. As warm surface currents are formed at low latitudes by strong insolation they are driven by winds, such as the Gulf Stream in the North Atlantic, moving this warm water to higher latitudes where they cool, become denser and sink, thus forming deep water. This Atlantic transition from surface waters to bottom waters is called the Atlantic Meridional Overturning Circulation (AMOC).

The northeastern North Atlantic is heated by the warm swift surface currents of the North Atlantic Drift, the northerly flowing current of the Gulf Stream. As warm waters from the Gulf of Mexico move north along the eastern seaboard of North America, they turn sharply to the east between 40–51°N (Rossby, 1996). The Gulf Stream brings warm surface currents to the northeastern North Atlantic, exceeding 20 Sv (20,000,000 m^3s^{-1}) as it crosses the Mid Atlantic Ridge at 1 m s^{-1} (Rossby, 1996). To the west of Continental Europe, the Gulf Stream bifurcates into the south-westerly flowing Canary Current (clockwise) which is a crucial component of the North Atlantic Gyre; and the north-easterly flowing North Atlantic Current (anticlockwise) which is a crucial component of the North Atlantic Subpolar Gyre (Rossby, 1996). The warm North Atlantic Current is composed of saline Mediterranean overflow waters and upper

eastern Atlantic Water that flow into the Nordic Seas, via the Rockall Trough, to the Faroe – Shetland Channel (Rossby, 1996; McCartney & Mauritzen, 2001; Pollard *et al*. 2004). The North Atlantic Current also splits into both the Irminger and Faroes Currents, with the Irminger Current flowing to the west of Iceland and the Faroes Current to east of Iceland, over the Iceland – Faroe Ridge (Figure 4) (Hakkinen & Rhines, 2009). The Irminger Current supplies dense saline (34.9–35 psu) and relatively warm (4–6°C) Atlantic Water to the East Greenland Current in the western flowing portion of the Subpolar Gyre, thus aiding the formation of North Atlantic Deep Water (Reynaud *et al*. 1995; Hakkinen & Rhines, 2009).

The North Atlantic and Faroes Currents continue poleward as a conduit of warm saline Atlantic Water through the Norwegian and Greenland Seas towards the Arctic Ocean as the Norwegian Atlantic Current (Poulain *et al*. 1996; Orvik & Niiler, 2002). It splits into a two-branch current, with the western branch heading into the Norwegian and then Greenland Seas, eventually recirculating and flowing southwest in the Fram Strait as a component of the Subpolar Gyre (Orvik & Skagsketh, 2005). The eastern branch flows along the Norwegian Shelf for 3500 km virtually as a barotropic shelf current and eventually enters both the Barents Sea and Arctic Ocean (Orvik & Skagsketh, 2005). The Norwegian Atlantic Current also develops into the West Spitsbergen Current in a clockwise flow around Svalbard, transporting warm saline Atlantic Water into the interior of the Arctic Ocean along the eastern margin of the Fram Strait at an average of 9.5 Sv (~78.5°N) (Haugan, 1999; Fahrbach *et al*. 2001). The warm and saline West Spitsbergen Current engenders that the Fram Strait is the northernmost ocean body to remain ice-free throughout the year (Haugan, 1999).

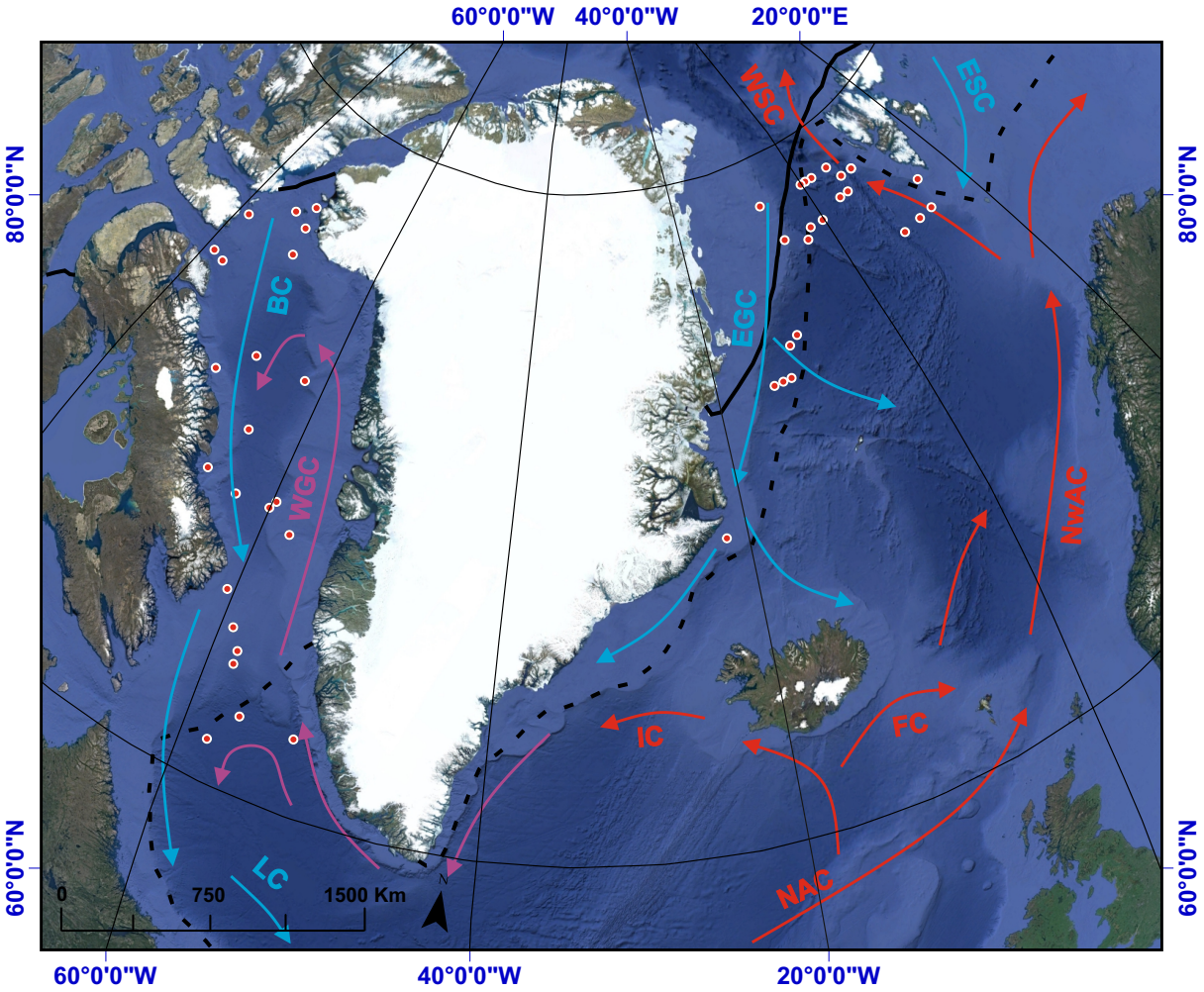

Figure 4: Projected coordinate system current and sea-ice extent map of the northern North Atlantic, with data point localities superimposed. Warm currents: NAC - North Atlantic Current, FC – Faroes Current, NwAC – Norwegian Atlantic Current, WSC – West Spitsbergen Current, IC – Irminger Current. Temperate current: WGC – West Greenland Current. Cold currents: ESC – East Spitsbergen Current, East Greenland Current, BC – Baffin Current, LC – Labrador Current. Dashed line: Winter sea-ice maximum (March) and continuous line: Summer sea-ice minimum (September) (Fetterer *et al*. 2018). Base map from Google Earth Pro.

The East Spitsbergen Current is comprised of cold and fresh Arctic Water originating from the Arctic Ocean and flowing through the Barents Sea around the eastern margin of Svalbard in a clockwise motion (Saloranta & Haugan, 2001). As the East Spitsbergen Current moves along the eastern coast of Svalbard it carries sea ice (seasonally) and has inputs from glaciers and river run off, additionally freshening the cold Arctic Water (Saloranta & Svendsen, 2001). Upon rounding the southwestern tip of Svalbard, the East Spitsbergen Current flows northwards along the continental shelf, parallel with the West Spitsbergen Current (flowing northwards along the continental slope) creating a boundary between the Arctic Water to the east and Atlantic Water to the west (Saloranta & Svendsen, 2001). In the western Fram Strait

along the Greenland continental margin, the East Greenland Current flows southwards transporting cold Arctic Water and sea ice at a rate of 21 Sv (Woodgate *et al*. 1999). There is a strong halocline, with ~0°C surface water having a salinity <30 psu, whereas at 150m depth the salinity is >34 psu (Aagaard & Coachman, 1968a) The sea-ice margin along the western and eastern margins of the Fram Strait are significantly further south than in the centre, primarily due to the transport of Atlantic Water by the West Spitsbergen Current. Ice export out of the Arctic Basin predominantly comes through the Fram Strait and the sea-ice concentrations of the Nordic Seas are related to this flux (Vinje, 2001; Sezerre *et al*. 2007)

The East Greenland Current is the most significant conduit of Arctic Water to the Nordic Sea's and northern North Atlantic, carrying deep and intermediate waters departing the Arctic Ocean and the western branch of Norwegian Atlantic Currents recirculating in the Fram Strait (Poulain *et al*. 1996; Orvik & Niiler, 2002; Rudels *et al*. 2002). The 640 m deep Denmark Strait crosses the Greenland-Iceland Ridge and is the primary channel for dense waters from the Nordic Seas to course into the northern North Atlantic, with channels along the Iceland-Faroe Ridge constituting the remainder (Mauritzen, 1996; Rudels *et al*. 2002; Jochumsen *et al*. 2015). Denmark Strait Overflow Water is a cold (<2°C) and saline (34.9 psu) gravity driven flow (with a gravity anomaly greater than 27.8 kg m^{-3}), that travels from the East Greenland continental shelf into the Irminger Basin, directed by topography (Dickson & Brown, 1994; Dickson *et* al. 2002; Tanhua *et al*. 2005; Jochumsen *et al*. 2015). The Denmark Strait Overflow Water at the Denmark Strait Sill is 3.4 Sv, before entering the abyssal subpolar North Atlantic as the bottom layer of the Deep Western Boundary Current (Jochumsen *et al*. 2012; Fischer *et al*. 2015). As the Deep Western Boundary Current travels southwest, the Denmark Strait Overflow Water and overriding Iceland Scotland Overflow Water and Irminger Current combine and become entrained so that the flow is 10.7 Sv near to Angmagssalik (Dickson *et al*. 2008; Häkkinen & Rhines, 2009). ~75% of the Denmark Strait Overflow Water found at Angmagssalik is sourced from north of the Denmark Strait and proceeds on to deep North Atlantic waters (Jochumsen *et al*. 2015). The southern flow of the AMOC is manifested by North Atlantic Deep Water at a depth between 1500 and 4000 m, with the northward flowing Antarctic Bottom Water below and surface return flow above (Antarctic Intermediate Water and warm surface waters) (Figure 5) (Hegerl & Bindoff, 2005).

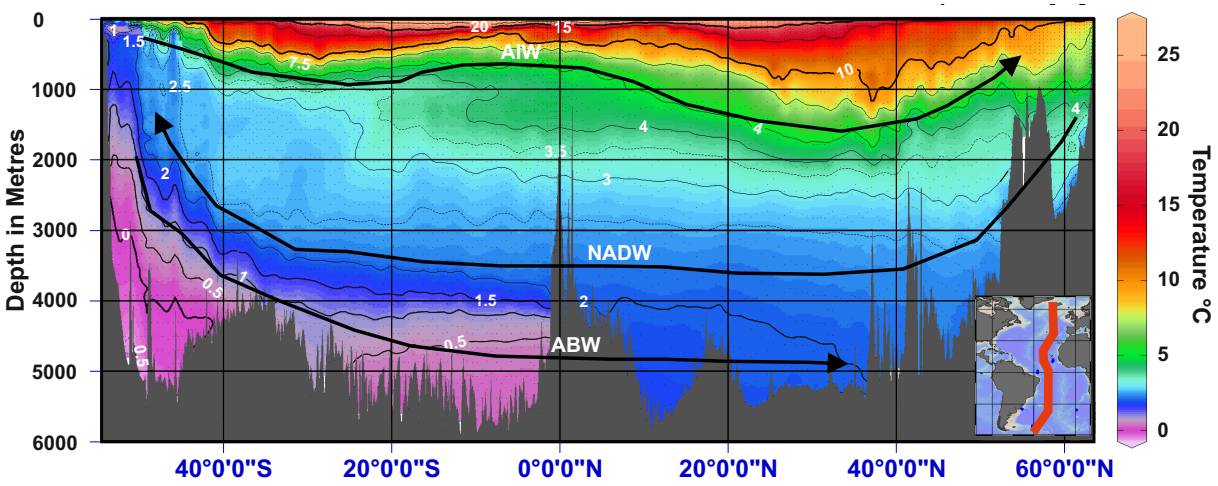

Figure 5: Cross section of the potential temperature of the Atlantic Ocean basin from ~55°S–65°N (map inset). ABW – Antarctic Bottom Water, NADW – North Atlantic Deep Water, AIW – Antarctic Intermediate Water and warm surface currents. Adapted from Schlitzer, (2003).

The West Greenland Current flows along the western margin of Greenland from Cape Farewell, as a continuation of the merged East Greenland and Irminger Currents in the cyclonic Subpolar gyre (Myers *et al*. 2009). The East Greenland and Irminger Currents become increasingly entrained as they move northwards as they are indistinguishable in velocity, but distinguishable in hydrographic properties (Fratantoni & Pickart, 2007; Oksman *et al*. 2017a). The West Greenland Current transports temperate and relatively fresh Arctic Water along the shelf edge northwards, whilst warmer and more saline (Irminger Current derived) Atlantic Waters flow offshore (Fratantoni & Pickart, 2007). In the northernmost Labrador Sea, the flow bifurcates with the majority flowing cyclonically around the Labrador Basin and the rest flowing northward into Baffin Bay along the Greenland shelf (Reverdin *et al*. 2003; Frantantoni & Pickart, 2007). The Arctic Water component of the West Greenland Current weakens at approximately 64°N, resulting in the relatively warmer Irminger Current derived Atlantic Water component to rise to the surface in central Baffin Bay and influence the West Greenland Current (Boertmann *et al*. 2013; Krawczyk *et al*. 2016; Oksman *et al*. 2017a). In northern Baffin Bay Arctic waters enter via the Robeson Channel in the Nares Strait in addition to the James and Lancaster Sounds (Tang *et al*. 2004). Consequently, cold Arctic Waters flow southwards along the western shelf edge in the Baffin Current, resulting in a large-scale anticlockwise gyre circulation in Baffin Bay, with the West Greenland Current being rerouted southwards (Oksman *et al.* 2017a). Icebergs calved from glaciers in western Greenland (primarily in Disko and Umanak Bays) and exceeding 1 million tons, have a propensity to travel

northwards along the West Greenland Current, cross northern Baffin Bay and then travel southwards along the Baffin Current, entering the Labrador Sea through the Davis Strait (Tang *et al*. 2004). Open water sea ice in Baffin Bay starts to form in September in the north and then steadily southwards until the entirety of Baffin Bay is frozen, except for the south-eastern Davis Strait, which is influenced by the temperate West Greenland Current (Tang *et al*. 2004).

The Baffin Current exits Baffin Bay through the Davis Strait into the northwestern Labrador Sea. It proceeds southward along the Labrador Shelf and is amalgamated with the Hudson Bay outflow and the cyclonically flowing portion of the West Greenland Current, forming the Labrador Current (Fratantoni & Pickart, 2007).

2.3. Sea ice extent

Maximum extent of Arctic sea ice usually occurs in March and in 2018 this covered 14.3 million km^2 (Fetterer *et al*. 2018). During the winter sea-ice maximum, the median ice edge (1981–2010) stretches to 75°N south of Svalbard in the Barents Sea and along the shelf west of Svalbard (Divine & Dick, 2006; Fetterer *et al*. 2018). Sea ice stretches from a narrow coastal belt in Cape Farewell (southernmost Greenland) northwards, on the eastern coast of Greenland; progressively thickening and eventually reaching up to 400 km into the Fram Strait until it reaches the eastern Fram Strait, where sea ice doesn't extend further south than 80°N (Divine & Dick, 2006). During the winter maximum sea-ice extent, Hudson Bay and Baffin Bay are entirely frozen down to 59°N in the southwest Davis Strait (Tang *et al*. 2004). In the eastern Davis Strait, sea-ice extends to 65°N with open ocean to the south (Tang *et al*. 2004; Fetterer *et al*. 2018). In northern Baffin Bay the North Water Polynya (Figure 2), a region of recurrent anomalously thin ice, occurs at the meeting point of Lancaster Sound, Jones Sound and the southern end of the Kane Basin, reaching up to 85,000 km^2 in area (Dunbar *et al*. 1969; Tang *et al*. 2004). During maximum sea-ice conditions ~10% is kept open by local winds, tides and a well delineated ice bridge at the southern margin of the Kane Basin (Tang *et al*. 2004). The primary control on keeping the North Water Polynya ice-free is the strong southward flow of Arctic Waters and ice in addition to minor inputs from the temperate West Greenland Current from the southeast although it has lost much heat through isopycnal

mixing with cold Arctic Waters (Melling *et al*. 2001). Upwelling of relatively warm water near the Greenland coast is entrained in brines in the ice, resulting in one-third of total sensible heat loss and thus delaying ice growth (Melling *et al*. 2001).

Arctic sea ice usually experiences its minimum extent during September and in 2018 this was 4.7 million km^2 (Fetterer *et al*. 2018). During the summer sea-ice minimum in the eastern Fram Strait and north of Svalbard and the Barents Sea, the median ice edge (1981–2010) is 81°N (Fetterer *et al*. 2018). Sea ice extends northwards from 73°N on the Greenland coastline, progressively reaching further seawards along the Greenland shelf (Divine & Dick, 2006). Baffin Bay is ice free during the summer sea-ice minimum, barring thin strips of sea-ice along the coastlines, particularly along Baffin Island (Tang *et al*. 2004). Sea ice is limited to the west of Devon Island and 78°N in the Kane Basin (Fetterer *et al*. 2018).

3. METHODOLOGY

3.1. Materials and Methods

To separate the diatom species grouped under *F. oceanica* from the training set of the northern North Atlantic (Andersen *et al*. 2004a, 2004b; Miettinen *et al*. 2015; Oksman *et al*. 2019) and count the crysophyte cyst *Archaeomonas* sp., it was necessary to amass the constituent slides from storage in the Norwegian Polar Institute. The slides underwent microscopic analysis in the laboratory of Biokeskus 3 at the Viikki Campus of Helsinki University.

Of the 183 surface sediment samples comprising the training set, 80 were collected before the 1990's by Koç Karpuz and Schrader (1990) as the original calibration dataset. A further 57 samples were collected by Birks and Koç (2002) between 1990–2000. The final 46 slides which were analysed for this study (Appendix 1) were collected between 2006–2008 by Miettinen *et al*. (2015). The training set utilised the weighted average partial least squares transfer function developed by Ter Braak and Juggins (1993) for the 52 diatom species analysed.

All 46 of the surface sediment slides were collected using either a box-corer or multi-corer during several cruises of the study area between 2006–2008 (Figure 1). The samples comprise the top 1 cm of the sediment. The modern environmental data for the surface sediment samples consisted of two elements: sea-surface temperature and sea-ice data. All of the sea-surface temperatures were collated from the World Ocean Atlas 2001 (Stephens *et al*. 2002). The sea-ice data was collated from the National Snow and Ice Data Center, utilising data from 1979–2006, 1979–2007 and 1979–2008 to correspond to the years the data was collected by Miettinen *et al*. (2015) (NSIDC, www.nsidc.com). Sea-ice data referred to in the discussion are April sea-ice concentrations and sea-surface temperatures referred to are August sea-surface temperatures, in line with the environmental variables selected for the RDA (Figure 9) and previous literature (Berner *et al*. 2008; Miettinen *et al*. 2015; Oksman *et al*. 2019).

The counting was undertaken with a ZEISS Axio Imager A2 microscope with immersion oil on slide at 1000x magnification, and photomicrographs were taken using the ZEN Blue software (Figures 6 and 7). A total of 100 diatom valves (halves of the diatom frustule) of the targeted species were counted per sample, with a maximum scope of 10 transects for slides with low abundances. The counts largely mirrored both the training set and downcore counts for the grouped *F. oceanica* in Miettinen *et al*. (2015). The chrysophyte cysts *Archaeomonas* sp. were counted independently from the total diatom counts.

The different species were identified from their characteristic differences:

- *Fragilariopsis reginae-jahniae* from the characteristic elongate, parallel and linear valve shape with thicker continuous striae (Jensen, 2003; Lundholm & Hasle, 2010). Apical axis ~40–60 µm, transapical axis ~5–6 µm with a distinctive nodule on the eccentric raphe (Witkowski *et al*. 2000; Jensen, 2003).
- *Fossula arctica* from the characteristic capitate ends and thin discontinuous striae. Larger valves are more elongate with capitate apices, whilst smaller valves are elliptical with rounded apices (Jensen, 2003). Apical axis ~8–50 µm, transapical axis ~5.5–7.5 µm (Hasle *et al*. 1996; Jensen, 2003).
- *Fragilariopsis oceanica* from the characteristic ellipsoidal to lanceolate shape with rounded apices and raphe with a central nodulus (Jensen, 2003). Apical axis ~26–43 µm, transapical axis ~4.5–6 µm (von Quillfeldt, 2001).

- The chrysophyte cysts *Archaeomonas* sp. resting stages were identified from their scabrate texture, sometimes visible pore, small spines (<5 µm) and total size of <10 µm (Perch-Nielsen, 1978).

3.2. Statistical analysis

The apparent relative abundances were assessed once all of the slides had been accounted for and the environmental data was applied to analyse species – environment relationships and their statistical significance. The environmental variables used were August sea surface temperature (hereinafter referred to as aSST) and April sea-ice concentration (hereinafter referred to as aSIC) based on previous literature applying the North Atlantic training set for downcore reconstructions (e.g. Berner *et al*. 2008; Miettinen *et al*. 2015).

Multivariate statistical analysis of the count data was undertaken with CANOCO version 5.01 software (Ter Braak & Šmilauer, 2012). The now separated three diatom species *Fragilariopsis oceanica, Fragilariopsis reginae-jahniae* and *Fossula arctica* were converted into percentages relative to what the grouped *F. oceanica* originally constituted in the assemblage (Miettinen *et al*. 2015). This allowed for the multivariate statistical analysis of the three species within the same North Atlantic training set. The chrysophyte cysts *Archaeomonas* sp. was additionally incorporated into the training set by adding its counts to the original training set counts and dividing the sum total by the number of chrysophyte cysts, generating a representative percentage. A redundancy analysis (hereinafter referred to as RDA) with a Monte Carlo permutation test (999 randomisations) was run for all the samples and expressed as a biplot of species against environmental variables with the chrysophyte cysts and grouped *F. oceanica* as supplementary variables (Figure 9). Based on the gradient length of the species data in detrended correspondence analysis (DCA; gradient length 1.8 SD units of species turnover), a linear method (RDA) instead of a unimodal method (canonical correspondence analysis, CCA) was selected.

Environmental response curves were created based on the species and environmental data (Figures 10–14) in conjunction with Stephen Juggins from Newcastle University. The numerical analyses were undertaken using R 3.4.1 software (R Core Team, 2017) with the

package eHOF, following the hierarchical response models used in Jansen & Oksanen (2013). The described model has seven variations of response: 1 – flat response; 2 – monotone sigmoid; 3 – monotone sigmoid with plateau; 4 – unimodal symmetric; 5 – unimodal skewed; 6 – bimodal with equal peaks; and 7 – bimodal with unequal peaks.

Further, the core MD99-2322 studied in Miettinen *et al*. (2015) was recounted (Appendix 2) to separate the three species, with the chrysophyte cysts *Archaeomonas* sp. counted additionally (Figure 16). The core was recounted for the Late Holocene time interval period ~690–1498 Common Era (hereinafter referred to as CE). The core was studied at a ~3 cm interval, yielding a temporal resolution of ~24 years and resulting in the counting of an additional 33 slides between 171 – 56 cm depth interval. The C2 program version 1.7 was used for turning the diatom counts into percentages and plotting them as a stratigraphical relative abundance diagram.

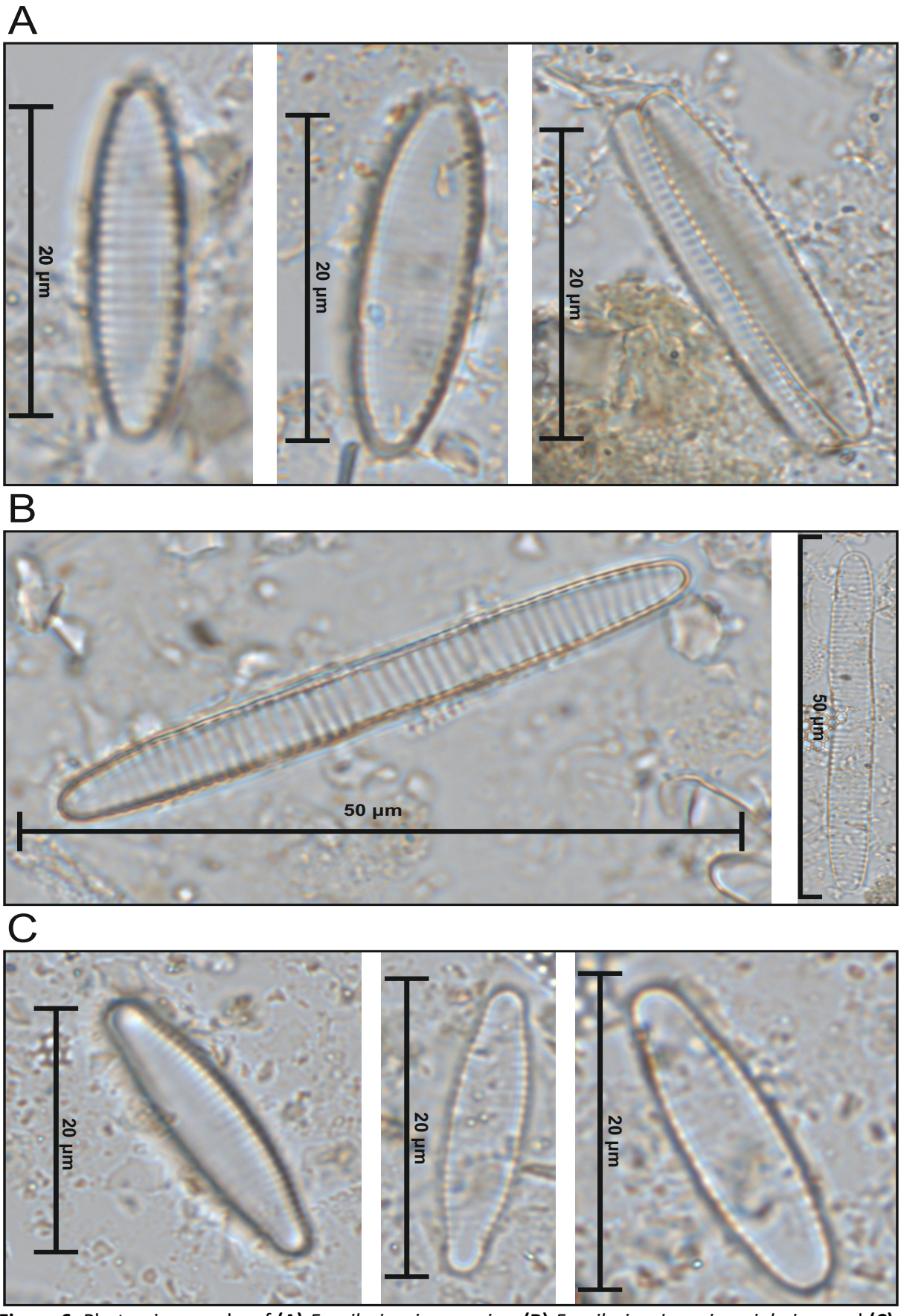

Figure 6: Photomicrographs of **(A)** *Fragilariopsis oceanica*; **(B)** *Fragilariopsis reginae-jahniae*; and **(C)** *Fossula arctica.* Images captured with a ZEISS Axio Imager A2 at 1000x magnification. Images from surface sediment slide HU2008-029-036 – North Atlantic, North Water Polynya.

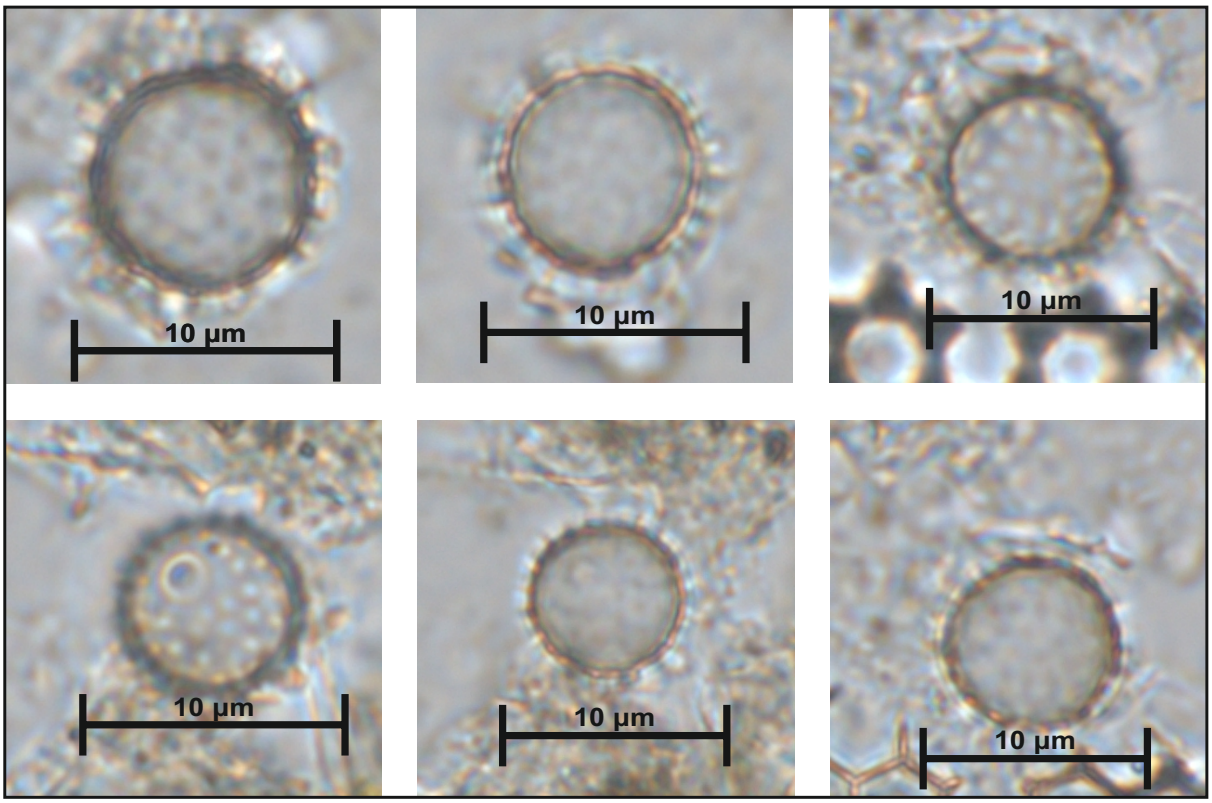

Figure 7: Photomicrographs of chrysophyte cysts. Images captured with a ZEISS Axio Imager A2 at 1000x magnification. Images from surface sediment slide HU2008-029-019 – North Atlantic, Baffin Bay.

4. RESULTS

4.1. Diatom species and *Archaeomonas* sp. relative abundances

Figure 8 indicates the relative abundances of the separated diatom species and chrysophyte cysts as percentages of total site assemblages in the training set from Miettinen *et al*. (2015). The abundance percentages are representative for the site in which the surface sediment sample was taken, as illustrated in Figure 1.

4.1.1. Fragilariopsis oceanica

Panel A in Figure 8 illustrates generally high abundances for *Fragilariopsis oceanica* across the entire northern North Atlantic, comprising from 0.49%–29.49% of total assemblages. East of Greenland, north of 75°N in the Fram Strait, there are 17 sites which vary in abundance between 3.09% and 18.62% and yield an average of 10.42%. South of 75°N in the Greenland

Sea are six sites, of which five are offshore and yield much lower abundances of 0.71%–3.45%. The nearshore site yields the highest abundance of the entire northern North Atlantic at 29.49%.

West of Greenland, in the Labrador Sea and Davis Strait south of 66°N, there are seven sites which vary in abundance from 0.74%–19.38% and yield an average of 6.82%. The nearshore site had the highest abundance. In Baffin Bay between 66°N and 72.5°N, there are nine sites which vary in abundance from 0.49%–7.2% and yield an average of 2.7%. In the northern margin of Baffin Bay and North Water Polynya north of 74°N there are seven sites which vary in abundance from 5.52%–22.59% and yield an average of 14.56%.

The highest abundances of *Fragilariopsis oceanica* tend to be north of 75°N east of Greenland, and north of 74°N west of Greenland. Two nearshore sites south of these latitudes also yielded high abundances east of Greenland (19.38%) and west of Greenland (29.49%), although other nearshore sites also had lower abundances west of Greenland (2.61% and 7.2%).

4.1.2. Fragilariopsis reginae-jahniae

Panel B in Figure 8 illustrates generally quite low to moderate abundances for *Fragilariopsis reginae-jahniae* across the northern North Atlantic, comprising from 0%–14.29% of total assemblages. East of Greenland in the Fram Strait north of 75°N, the 17 sites vary in abundance from 0.36%–7.28% and yield an average of 3.07%. South of 75°N in the Greenland Sea the five offshore sites yield very low abundances of 0%–1.27%, with two of the sites registering 0%. The nearshore site yields a higher abundance of 5.51%.

West of Greenland, in the Labrador Sea and Davis Strait south of 66°N, the seven sites vary in abundance from 0%–14.29% (one site registering 0%) and yield an average of 2.91%. The nearshore site yielded 14.29%, whereas the six other sites had low abundances varying from 0%–4.36%. In Baffin Bay between 66°N and 72.5°N, the nine sites vary in abundance from 0.29%–7.2% and yield an average of 1.78%. In the northern margin of Baffin Bay and the North

Water Polynya north of 74°N, the seven sites vary in abundance from 4.13%–9.68% and yield an average of 6.95%.

The highest abundances of *Fragilariopsis reginae-jahniae* were found west of Greenland north of 74°N in the North Water Polynya region. The second highest abundances were found north of 75°N to the east of Greenland. High abundances occurred at nearshore sites south of 75°N to the east of Greenland (5.51%) and south of 66°N to the west of Greenland (14.29%).

4.1.3. Fossula arctica

Panel C in Figure 8 illustrates a range of low to high abundances for *Fossula arctica* across the northern North Atlantic, comprising from 0%–26.4% of total assemblages. East of Greenland in the Fram Strait north of 75°N the 17 sites vary in abundance from 0%–4.39% (one site averaging 0%) and yield an average of 1.71%. South of 75°N in the Greenland Sea, the five offshore sites yield low abundances of 0.63%–2.68%. The nearshore site yields a slightly higher abundance of 3.88%.

West of Greenland, in the Labrador Sea and Davis Strait south of 66°N, the seven sites vary in abundance from 0%–6.35% (one site registering 0%) and yield an average of 1.33%. The nearshore site yielded 6.35%, whereas the six offshore sites had low abundances varying from 0%–1.1%. In Baffin Bay between 66°N and 72.5°N, the nine sites vary from 0%–8.96% (two sites registering 0%) and yield an average of 1.83%. One nearshore site yielded 8.96%, whereas the other eight sites had low abundances varying from 0%–2.43%, including another nearshore site yielding 1.56%. In the northern margin of Baffin Bay and the North Water Polynya north of 74°N, the seven sites vary in abundance from 1.83%–26.4% and yield an average of 18.52%. Excluding the anomalously low site yielding 1.83%, the eight other sites had high abundances varying from 13.78%–26.4%

The highest abundances of *Fossula arctica* were found north of 74°N in northern Baffin Bay and the North Water Polynya. Abundances were consistently low at other sites in the

northern North Atlantic (<5%) except for the nearshore site in the Davis Strait (6.35%) and a nearshore site in Baffin Bay south of 72.5°N (8.96%).

4.1.4. Chrysophyte cyst *Archaeomonas* sp.

Panel D in Figure 8 illustrates high to very high abundances for *Archaeomonas* sp. across the northern North Atlantic, comprising from 1.56%–42.7% relative to total percentages. East of Greenland in the Fram Strait north of 75°N the 17 sites vary in abundance from 3.28%–23.04% and yield an average of 11%. South of 75°N in the Greenland Sea, the six sites (nearshore and offshore) vary in abundance from 7.26%–10.96% and yield an average of 8.95%.

West of Greenland, in the Labrador Sea and Davis Strait south of 66°N, the seven sites vary in abundance from 1.56%–8.56% and yield an average of 4.99%. These are the lowest abundances of *Archaeomonas* sp. in the northern North Atlantic. In Baffin Bay between 66°N and 72.5°N, the nine sites vary in abundance from 5.51%–42.7% and yield an average of 18.48%. In the northern margin of Baffin Bay and the North Water Polynya north of 74°N, the seven sites vary in abundance from 5.81%–14.41% and yield an average of 8.67%.

Archaeomonas sp. was abundant across the whole northern North Atlantic, with the highest concentrations occurring in Baffin Bay between 66°N and 72.5°N where three sites yielded high to very high abundances (23.95%, 30.37% and 42.7%). The second highest abundances were found north of 75°N in the Fram Strait where five sites had high abundances (>15%).

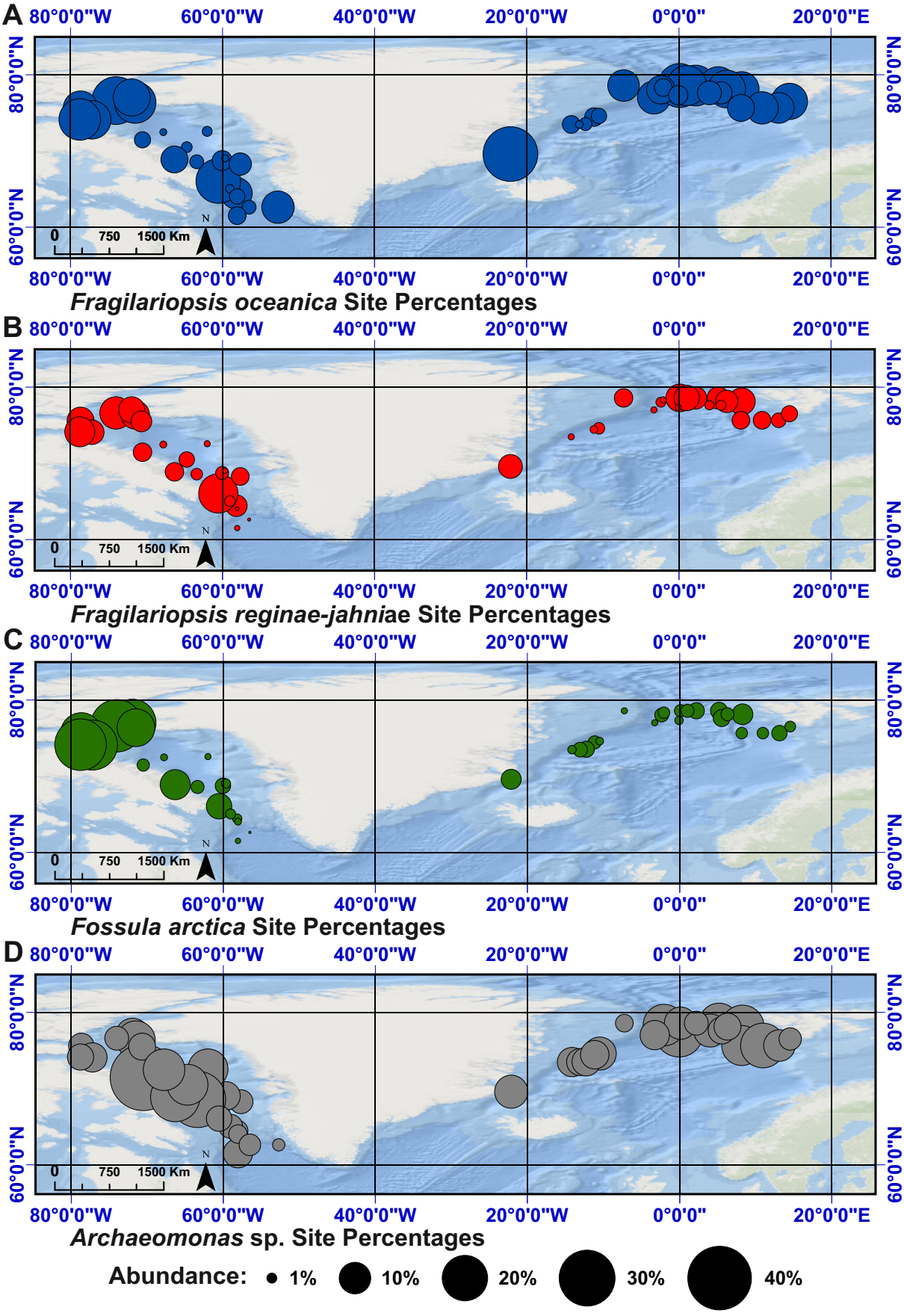

Figure 8: Relative abundances of **(A)** *Fragilariopsis oceanica*; **(B)** *Fragilariopsis reginae-jahniae*; **(C)** *Fossula arctica*; and **(D)** *Archeomonas* sp. expressed as a percentage per locality. Base map from ESRI.

4.2. Redundancy analysis (RDA)

Of the original 52 diatom species in the training set, 14 species had a 0% abundance and were removed from analysis. With the separation of *Fossula arctica* and *Fragilariopsis reginae-jahniae* and addition of the chrysophyte cyst *Archaeomonas* sp., the remaining 38 species present in the analysed surface sediment samples increased to 41 species. The 21 most common bioindicator species of the northern North Atlantic used in Oksman *et al*. (2019) are expressed on the biplot in addition to the separated species and chrysophyte cysts.

In the RDA, the two explanatory variables (aSST and aSIC) account for 25.6% of the total variance in the diatom data. The first axis accounts for 17.29% of this explained variation (cumulative), with the second axis accounting for a further 8.31%. The *p* – value of 0.001 indicates strong evidence against the null hypothesis. The analysis displays the strong aSST/aSIC gradient that diagonally represents axes 1 and 2. The ecologies of the 21 species and their relation to aSIC and aSST is described in Oksman *et al*. (2019). This variation is evident from the scattered plotting of the different species, with 'open marine' species gravitating to the high end of the aSST variable and sea-ice species gravitating to the high end of the aSIC variable. Species which do not gravitate to either variable and plot in the centre of the biplot are 'Intermediate' species.

Sea-ice species plotting to the left of axis 1 and below axis 2 are represented by: *Actinocyclus curvatulus*, *Coscinodiscus oculus-iridis, Fossula arctica*, *Fragilariopsis cylindrus, Fragilariopsis oceanica* (grouped), *Fragilariopsis reginae-jahniae*, *Porosira glacialis* and *Thalassiosira antarctica* var. *borealis* spore.

'Cold-intermediate water species plotting to the right of axis 1 and below or directly on axis 2 are represented by: chrysophyte cyst *Archaeomonas* sp., *Fragilariopsis oceanica* (separated), *Rhizosolenia hebetata* f. *hebetata*, *Thalassiosira anguste-lineata* and *Shionodiscus trifultus*.

'Temperate-mixed' water species plotting to the right of axis 1 and above axis 2 are represented by: *Bacterosira bathyomphala*, *Coscinodiscus radiatus*, *Thalassiotrix longissima*, *Thalassiosira hyalina* and *Thalassiosira nordenskioeldii.*

Open marine species plotting to the left of axis 1 and above axis 2 are represented by: *Coscinodiscus marginatus*, *Rhizosolenia hebetata* f. *semispina*, *Thalassionema nitzschioides*, *Thalassiosira angulata*, *Thalassiosira gravida*, *Shionodiscus oestrupii* and *Thalassiosira pacifica*.

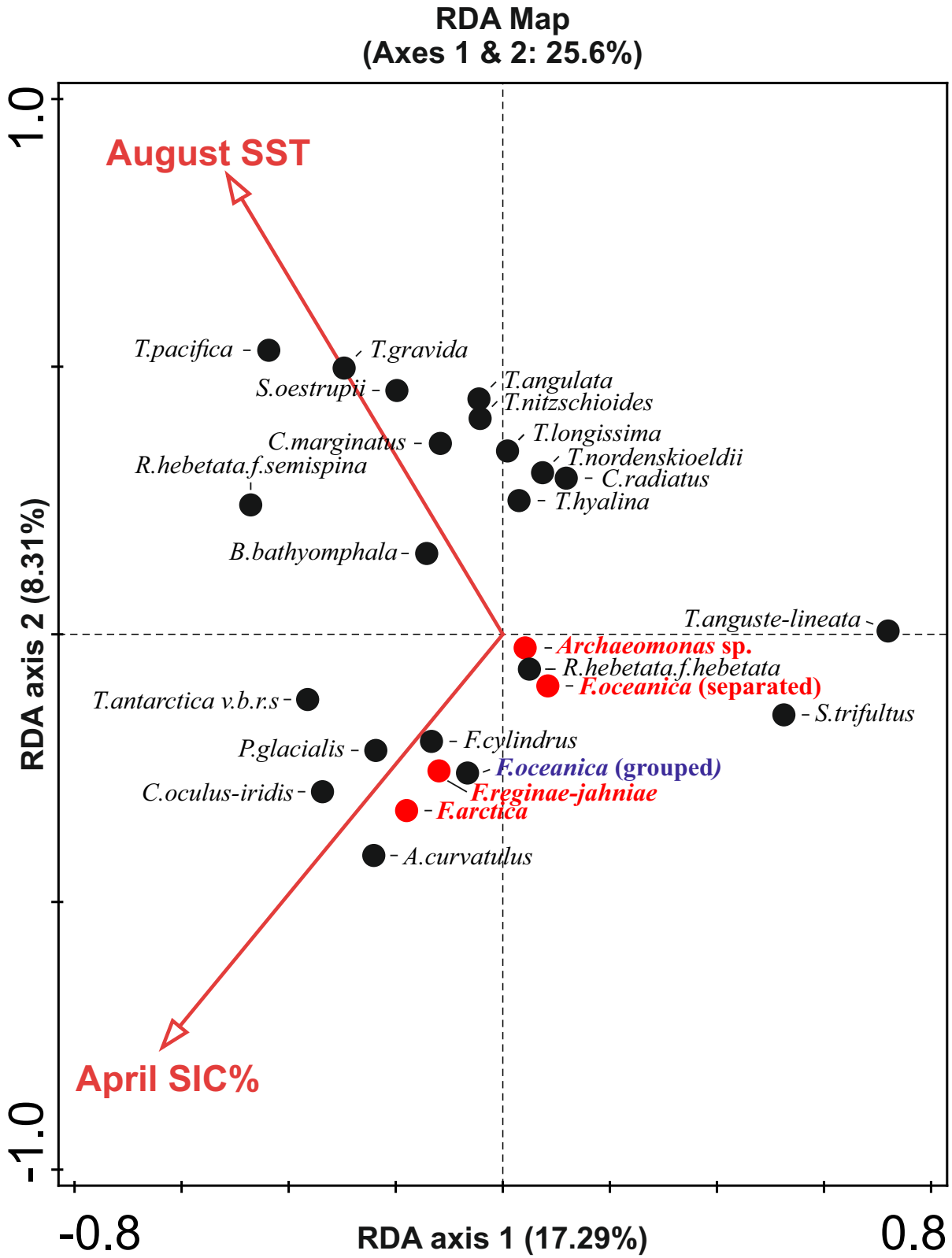

Figure 9: Species biplot of the 21 most common high latitude diatom species (in black), the grouped *F. oceanica* (in purple), the separated diatom species and chrysophyte cysts (in red) and environmental variables April sea-ice concentration and August sea-surface temperature. A redundancy analysis (RDA) was run for all samples using Canoco version 5.1 (Ter Braak & Šmilauer, 2012).

4.3. Environmental response curves

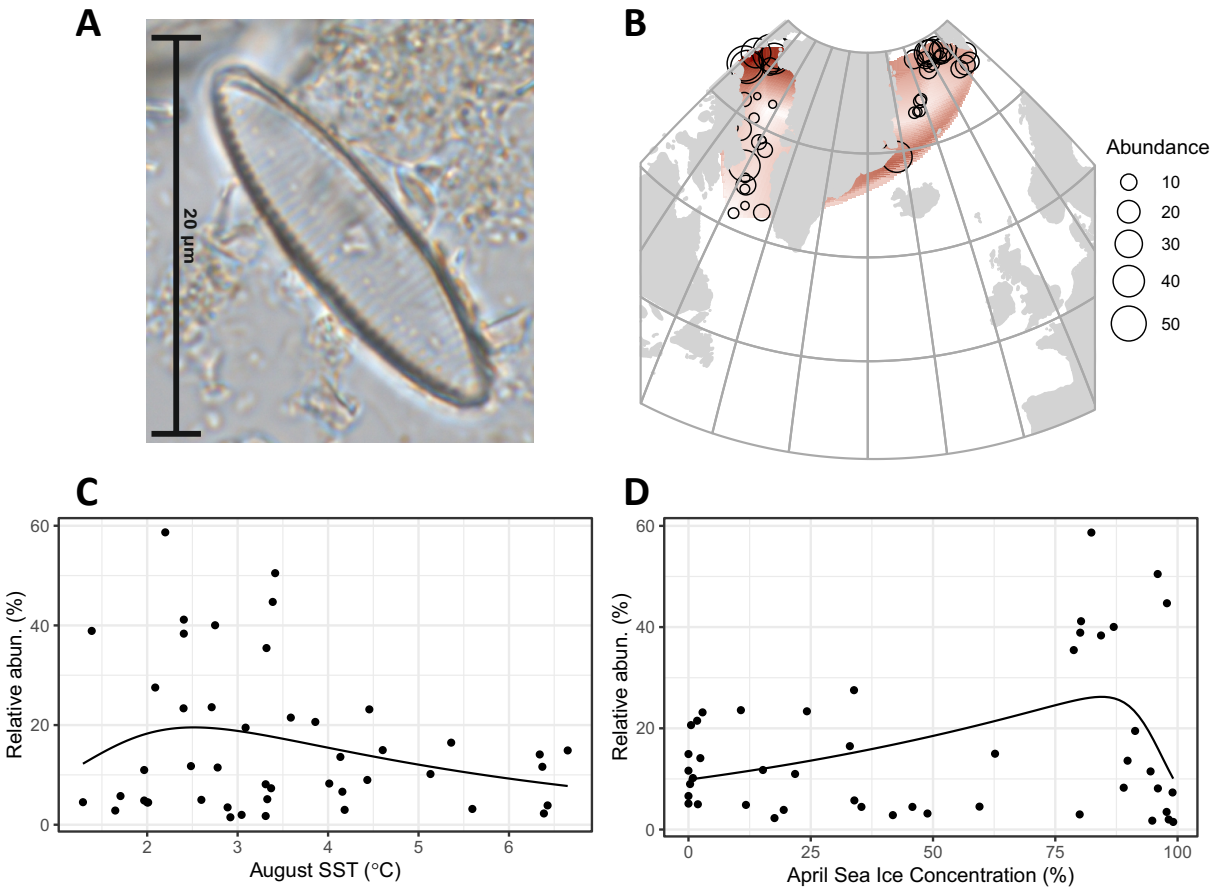

Figure 10: *Fragilariopsis oceanica* (grouped). **(A)** Photomicrograph of the species; **(B)** Geographical distribution; **(C)** Response curve to August sea-surface temperatures; **(D)** Response curve to April sea-ice concentrations. Created in conjunction with Stephen Juggins, Newcastle University.

Response to environmental gradients: Temperature range between 1.2°C–6.6°C, with an aSST optimum of 2.5°C (Figure 10, Panel C). Highest abundances found above 75% aSIC (Figure 10, Panel D). Statistically significant relationship to both sea surface temperature (unimodal skewed) and sea-ice concentration (unimodal skewed).

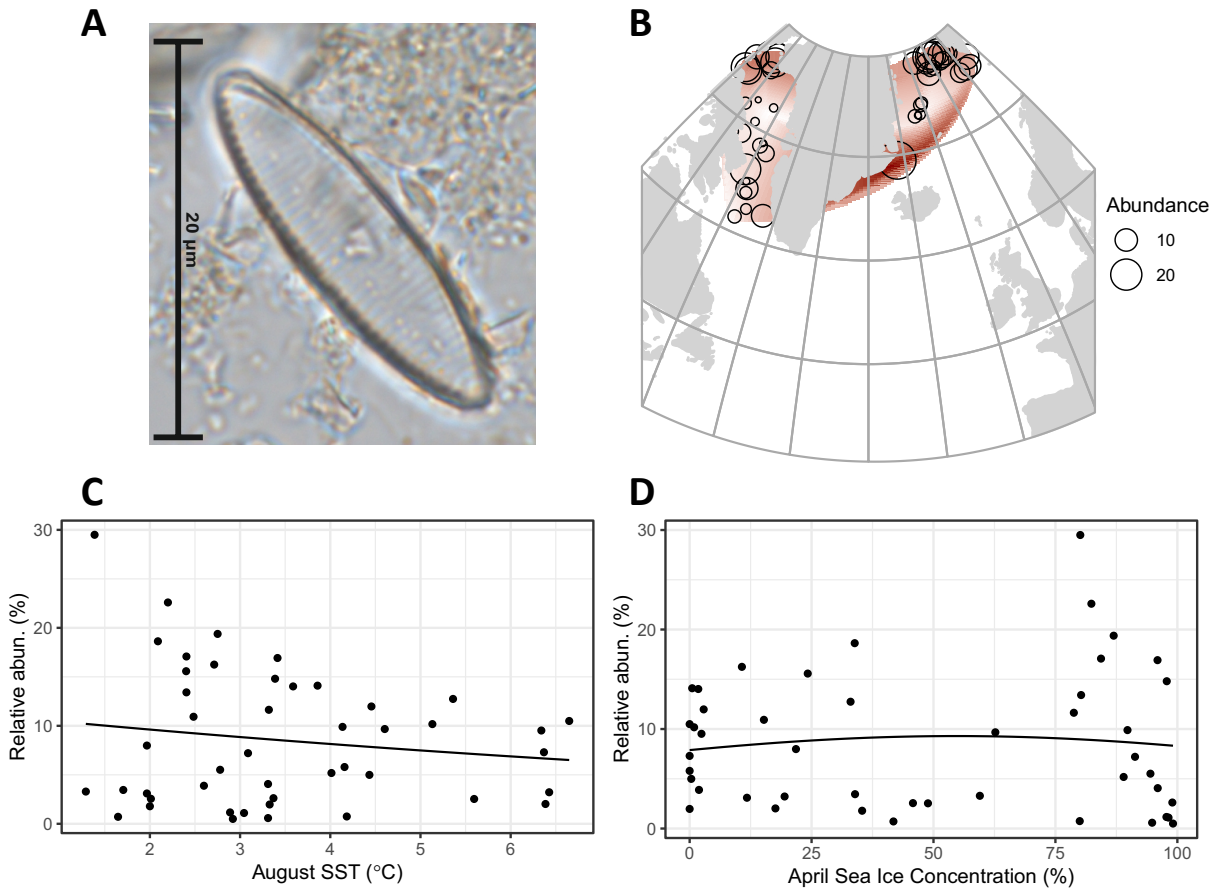

Figure 11: *Fragilariopsis oceanica* (separated). **(A)** Photomicrograph of the species; **(B)** Geographical distribution; **(C)** Response curve to August sea-surface temperatures; **(D)** Response curve to April sea-ice concentrations. Created in conjunction with Stephen Juggins, Newcastle University.

Response to environmental gradients: Temperature range between 1.2°C–6.6°C, with an aSST optimum of <4°C (Figure 11, Panel C). Highest abundances found above 75% aSIC in addition to below 30% (Figure 11, Panel D). Statistically significant relationship to both sea surface temperature (monotone sigmoid) and sea-ice concentration (monotone sigmoid).

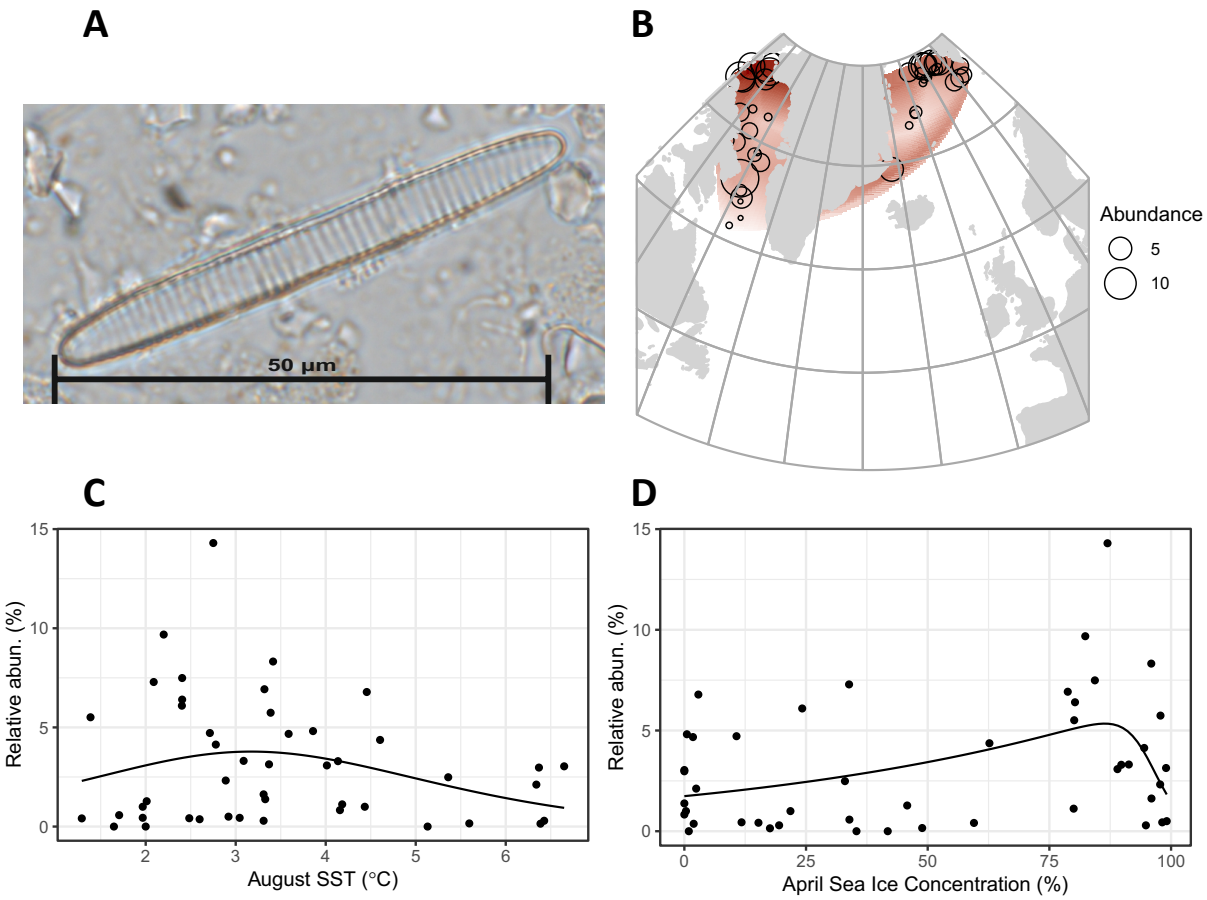

Figure 12: *Fragilariopsis reginae-jahniae*. **(A)** Photomicrograph of the species; **(B)** Geographical distribution; **(C)** Response curve to August sea-surface temperatures; **(D)** Response curve to April sea-ice concentrations. Created in conjunction with Stephen Juggins, Newcastle University.

Response to environmental gradients: Temperature range between 1.2°C–6.6°C, with an aSST optimum of 3°C (Figure 12, Panel C). Highest abundances found above 75% aSIC (Figure 12, Panel D). Statistically significant relationship to both sea surface temperature (unimodal symmetric) and sea-ice concentration (unimodal skewed).

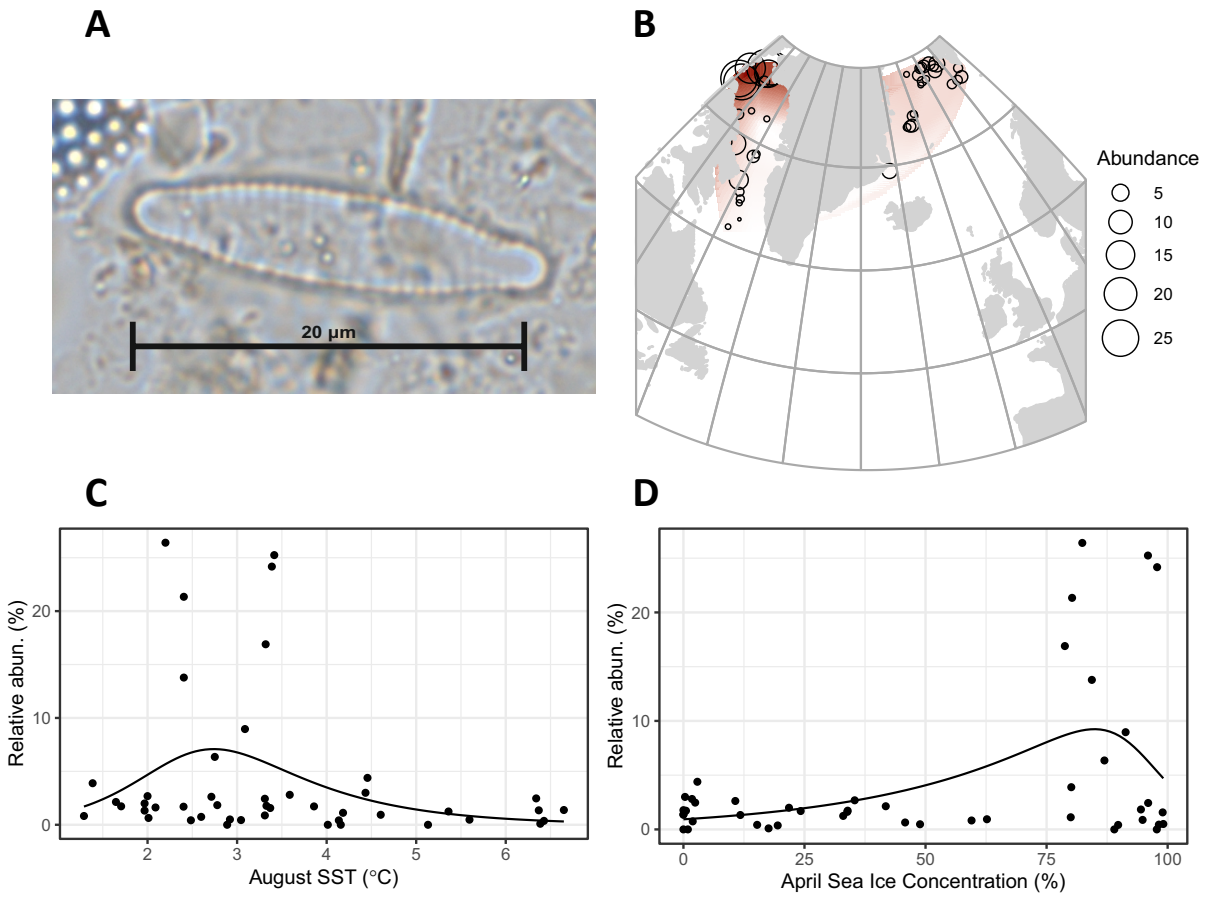

Figure 13: *Fossula arctica*. **(A)** Photomicrograph of the species; **(B)** Geographical distribution; **(C)** Response curve to August sea-surface temperatures; **(D)** Response curve to April sea-ice concentrations. Created in conjunction with Stephen Juggins, Newcastle University.

Response to environmental gradients: Temperature range between 1.2°C–6.6°C, with an aSST optimum of 2.6°C (Figure 13, Panel C). Highest abundances found above 75% aSIC (Figure 13, Panel D). Statistically significant relationship to both sea surface temperature (unimodal skewed) and sea-ice concentration (unimodal skewed).

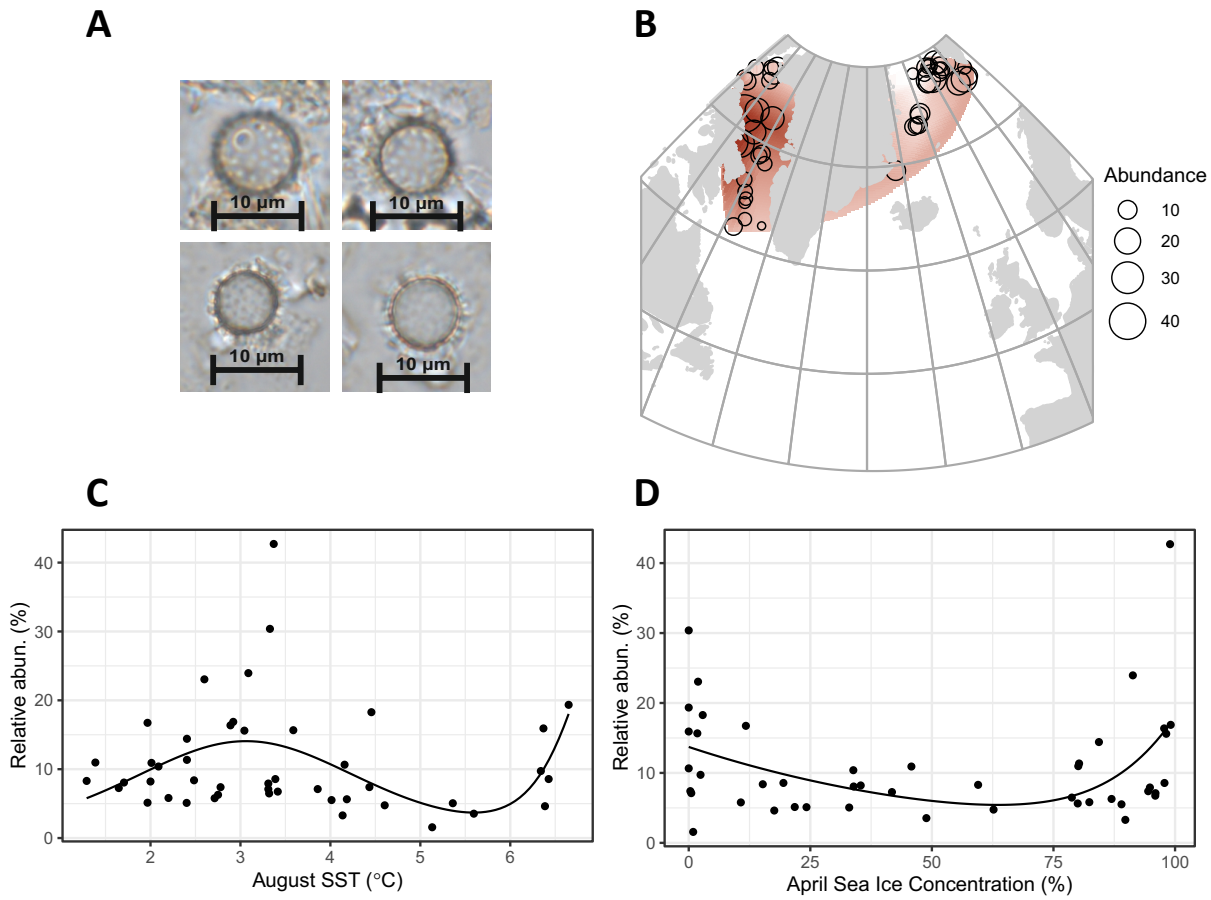

Figure 14: Chrysophyte cyst *Archaeomonas* sp. **(A)** Photomicrographs of the species; **(B)** Geographical distribution; **(C)** Response curve to August sea-surface temperatures; **(D)** Response curve to April sea-ice concentrations. Created in conjunction with Stephen Juggins, Newcastle University.

Response to environmental gradients: Temperature range between 1.2°C–6.6°C, with a bimodal aSST optimum of 3°C and 6.6°C (Figure 14, Panel C). Highest abundances found above 75% aSIC and in ice free conditions (Figure 14, Panel D). Statistically significant relationship to both sea surface temperature (bimodal with equal peaks) and sea-ice concentration (bimodal with equal peaks).

4.4. Downcore diatom and *Archaeomonas* sp. analysis

The core MD99-2322 was analysed from 171 cm to 56 cm depth, corresponding to the time period ~690–1498 CE. The total number of diatom frustules counted per slide for Miettinen *et al*. (2015) was 300 or more, of which the most abundant high-latitude species are illustrated as percentages in Figure 15. The grouped *F. oceanica* is one of the most dominant species in the assemblage alongside *T. gravida*, *R. hebetata.* F. *hebetata, T. nordenskioeldii, T. hyalina* and *B. bathyomphala*.

From ~690–994 CE the relative abundance of *F. oceanica* is high at over 20% with a maximum abundance of 29.3% at ~934 CE, with only a small decrease to 14.6% by ~873 CE. Following a high abundance of 28.9% at ~976 CE the relative abundance fell sharply to 10.1% by ~1013 CE, with an ephemeral increase to 19.9% occurring by ~1116 CE and decreasing to 13.6% by ~1134 CE. Relative abundances then fell below 10%, with a small increase to 12% occurring by ~1188 CE. Relative abundances then fell again and remained constantly below 10% until ~1498 CE, with a minimum abundance of 1.9% occurring at ~1397 CE.

The separated assemblage illustrated in Figure 16 indicate that *F. arctica* and *F. reginae-jahniae* have very low abundances, consistently below 2% and 4% respectively. Conversely, *Archaeomonas* sp. yield a range of low to high abundances between 3% and 18%. The *F. oceanica* abundance appears to be largely unaffected by the separation into three species as the abundances of the other species were low.

The abundance of *F. arctica* is near its peak for the core at 1.3% at ~690 CE, decreasing slightly to 0.9% by ~916 CE and then increasing to the maximum abundance of 1.7% at ~934 CE. The relative abundance then decreases to 0.5% by ~976 CE, increasing to 1.1% at ~994 CE, then further decreases to 0.4% by ~1031 CE. A slight increase to 0.9% occurs by ~1055 CE, and only slightly decreases to 0.6% at ~1116 CE. A decrease to the minimum abundance of 0.1% occurs between ~1134–1152 CE, before a sharp increase to 1.6% by ~1188 CE. A decrease to 0.2% occurs between ~1296–1316 CE, followed by a slight increase to 0.7% by ~1377 CE. A decrease back to the minimum abundance of 0.1% occurs at ~1397 CE, followed by an increase to 0.5%

by ~1417 CE. This increase continues to 1% by ~1464 CE, before a decrease to 0.5% by ~1498 CE.

The abundance of *F. reginae-jahniae* is near its peak for the core at 3% at ~690 CE, decreasing to 1.4% by ~873 CE, then increasing to 2.6% by ~891 CE. A decrease to 1.7% by ~916 CE occurs before increasing again to the maximum abundance of 3.8% at ~934 CE. A decrease to 0.5% by ~1091 CE occurs before increasing to 1.8% by ~1116 CE. A decrease to 0.3% by ~1152 CE is followed by an increase to 1.1% by ~1215 CE. A decrease to 0.2% by ~1228 CE is followed by low abundances below 0.4% until ~1316 CE, when abundance increase to 3.2% by ~1350 CE. A sharp decrease to the minimum abundance of 0.1% at ~1397 CE follows and increases slightly to 0.5% by ~1498 CE.

The abundance of the separated *F. oceanica* is also high, with 18.3% at ~690 CE decreasing to 11.7% by ~873 CE and subsequently increasing to a maximum abundance of 26% at ~994 CE. A decrease to 8.5% by ~1013 CE follows, further decreasing to 6.9% by ~1091 CE with a subsequent sharp increase to 17.5% at ~1116 CE. A decrease to 7.2% by ~1152 CE occurs, followed by an increase to 9.4% by ~1188 CE. Abundances remain below 5% from ~1228 CE, with two minor peaks to 6.4% and 6% at ~1329 CE and ~1377 CE. The minimum abundance of 1.6% occurs at ~1397 CE.

The abundance of chrysophyte cysts throughout the core is high, but relatively muted at 7.3% at ~690 CE and decreasing to 5.7% by ~891 CE. An increase to 8.7% by ~976 CE is followed by a decrease to 7.6% by ~1013 CE. A significant increase to 13.7% at ~1055 CE is followed by a significant decrease to the minimum abundance of 3.2% at ~1134 CE. An increase to 9.6% by ~1170 CE is followed by a decrease to 5.5% by ~1188 CE, subsequently followed by an immediate increase to 12.7% by ~1215 CE. Abundances remain high, with a slight decrease to 11.7% from ~1275–1296 CE followed by the maximum abundance of 16.8% occurring at ~1329 CE. A slight decrease to 11.5% by ~1417 CE is followed by a further decrease to 10.5% by 1464, before an increase to 16% at ~1484 CE.

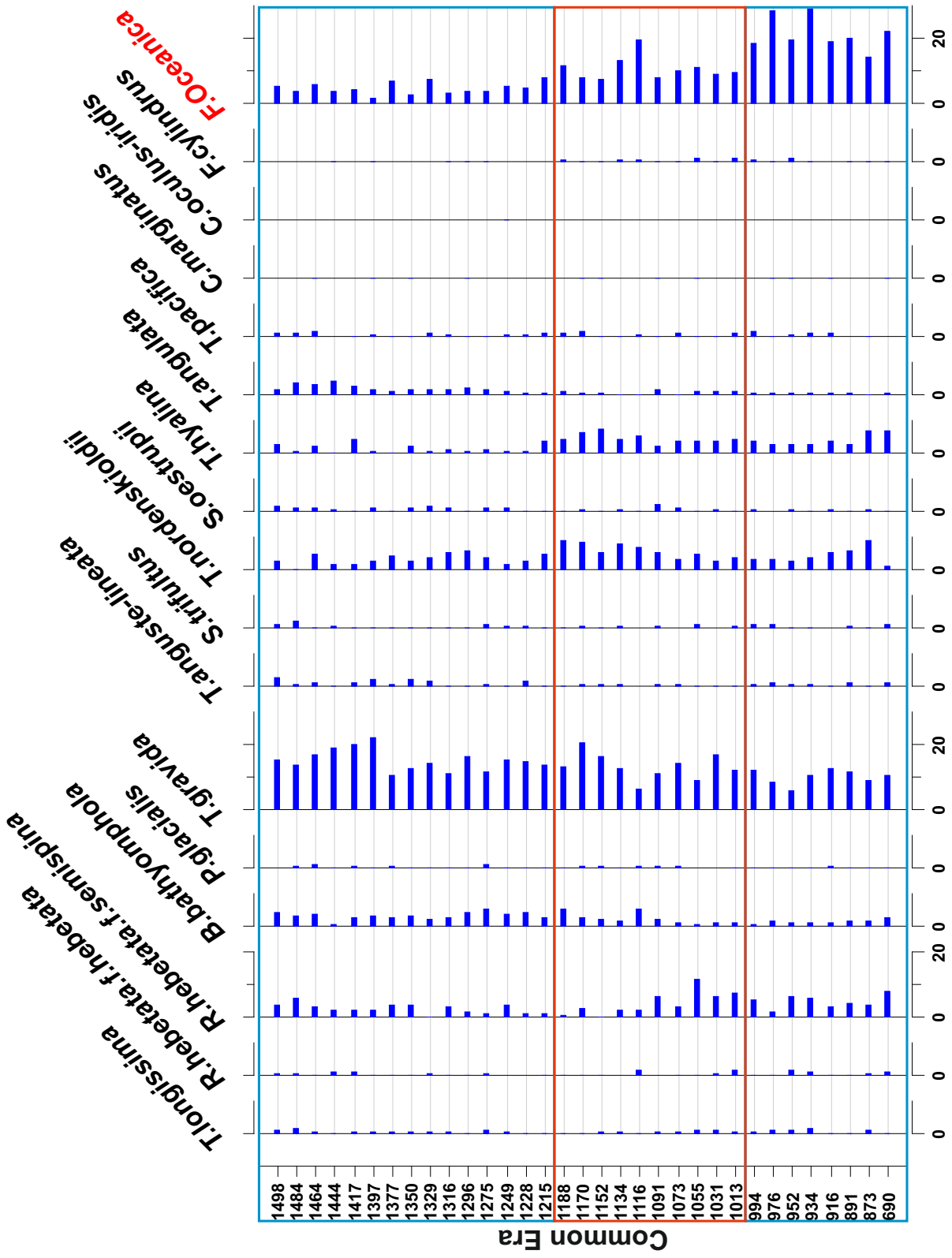

Figure 15: Downcore grouped diatom assemblage from site MD99-2322. Original grouped counts from Miettinen *et al*. (2015). Created using C2 software version 1.7 (Juggins, 2014).

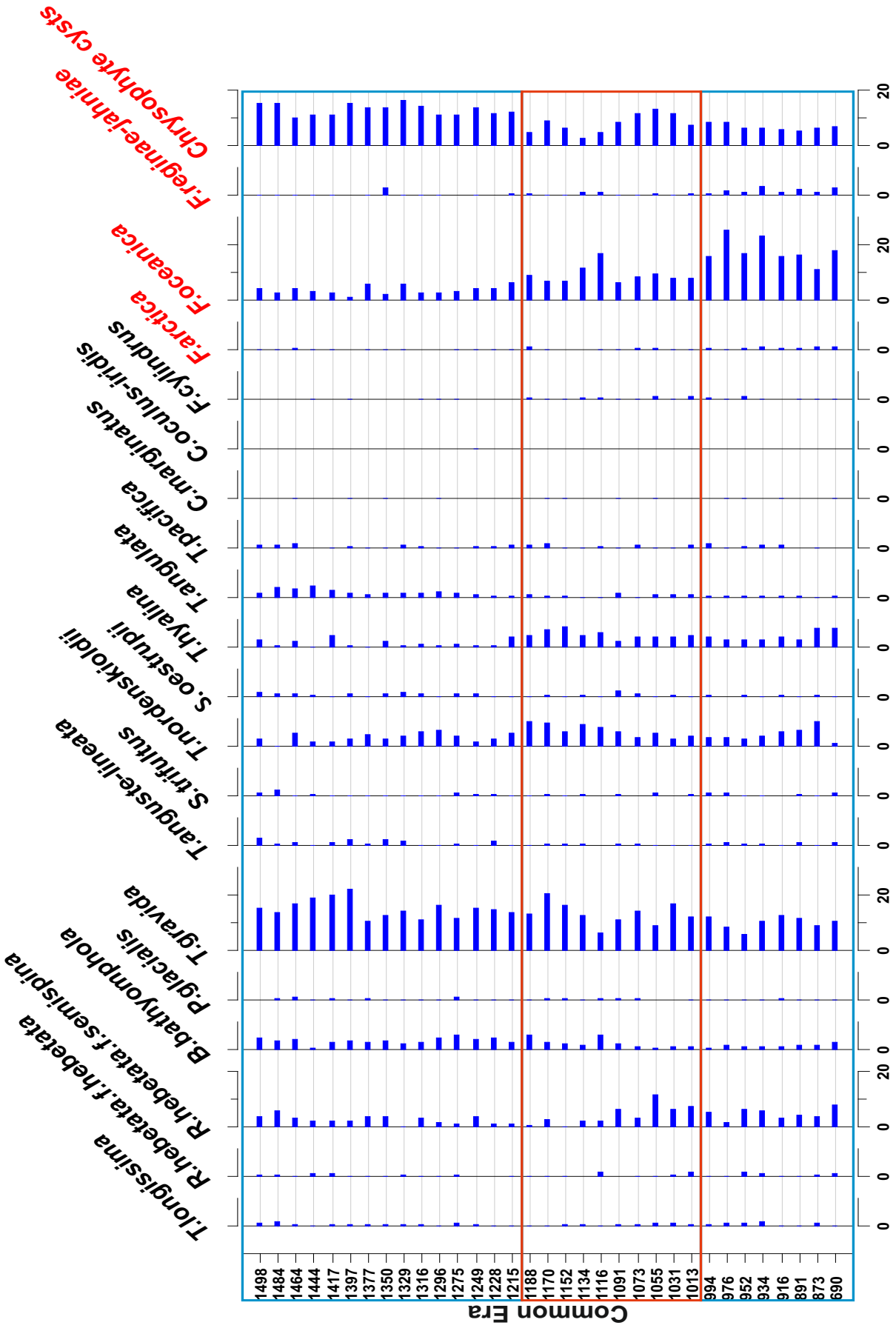

Figure 16: Downcore separated diatom assemblage and cysts from site MD99-2322. Separated from Miettinen *et al*. (2015). Created using C2 software version 1.7 (Juggins, 2014).

5. DISCUSSION

5.1. Species distribution and ecology

The grouped *F. oceanica* from Oksman *et al*. (2019) incorporated *F. arctica* and *F. reginae-jahniae* as 'sea-ice associated species' which potentially skewed the true response of *F. oceanica* to the environmental gradients aSST and aSIC. The separated diatom species analysed here exhibit heterogeneous distributions across the northern North Atlantic, with individual maximum abundances occurring in different regions with different aSST and aSIC (Figure 8). This indicates that separating the species to elucidate their relationships to both environmental gradients may qualitatively exemplify their ecologies. The separated species are described as reflecting the cold, low surface salinity conditions of the MIZ in Limoges *et al*. (2018); further statistical analyses may quantitatively enhance these ecological findings. The grouped *F. oceanica* was present at a temperature gradient from 1.2–6.6°C and had a statistically significant relationship to both aSST with highest abundances at 2.5°C aSST, and to aSIC with highest abundances at >75% aSIC (Figure 10). The grouped *F. oceanica* plotted amongst the sea-ice species in the RDA, indicating a relation to high aSIC (Figure 9).

The abundance of the separated *F. oceanica* is relatively high across the whole North Atlantic, averaging in excess of 10% above 75°N in the northern Greenland Sea and in excess of 14% above 74°N in Baffin Bay (Figure 8). The Greenland Sea is characterised by the dichotomous temperature gradient of the warm Atlantic Water dominated Norwegian Atlantic Current and West Spitsbergen Current to the east (Haugan, 1999) with relatively high average aSST (4.9°C), and the cold Arctic Water dominated East Greenland Current to the west with low aSST (2.4°C) (Woodgate *et al*. 1999) (Figure 4). In the central Fram Strait and Storfjord Through moderate to high abundances of *F. oceanica* (9.5%–16.2%) occurred in regions of open water with very low aSIC (0%–10.7%). To the east and closer to Svalbard, the cold and fresh East Spitsbergen Current ensures higher aSIC (32.9%) at the Hornsund Through which yielded analogous abundances of *F. oceanica* (12.7%) (Saloranta & Svendsen, 2001). The West Spitsbergen Slope to the north is far enough away from shore that the West Spitsbergen Current is dominant, with low aSIC (0.5%–2.8%) and abundances of *F. oceanica* (11.9%–14%) are also analogous. Along the East Greenland Margin the cold East Greenland Current

accommodates sea-ice formation much further to the south than in the eastern Fram Strait. Higher aSIC (15.2%–33.8%) from the West Fram Strait sea-ice edge had slightly higher abundances of *F. oceanica* (10.9%–18.6%). Further northwest, on the Greenland Shelf a site with very high aSIC (89.7%) also had comparable, but slightly lower abundances of *F. oceanica* (9.8%).

South of 75°N in the Greenland Sea, the cold-water sites along the East Greenland Margin and West Fram Strait sea-ice edge had moderate to high aSIC (33.9%–59.5%) and very low aSST (1.6°C), but low abundances of *F. oceanica* (0.7%–3.4%). The nearshore site located on the Scoresby Sound Shelf had very high aSIC (80%) and the highest abundance of *F. oceanica* (29.4%) recorded for the 46 re-analysed samples of the training set. The outflow of fresh glacier meltwater from the 38,000 km^2 system of fjords may play a significant role for this anomalously high abundance (Digby, 1953).

To the west of Greenland, the West Greenland and Irminger Currents transport temperate and fresh Atlantic Water northwards (Fratantoni & Pickart, 2007; Oksman *et al*. 2017a). In the eastern Labrador Sea south of 66°N the aSIC is very low (0.9%), but *F. oceanica* is relatively abundant (10.1%). Northwards, in the Davis Strait aSIC is significantly higher (62.68%) and *F. oceanica* is uniformly abundant (9.6%) while average aSST is relatively high (5.3°C). Other sites in the northern Labrador Sea and southerly Davis Strait have relatively moderate to very high aSIC (17.5%–79.9%) but the *F. oceanica* abundance is generally very low (0.7%–3.2%). The Baffin Current transports cold Arctic Water and oftentimes icebergs along the western margin of the Davis Strait (Oksman *et al.* 2017a). A nearshore cold-water site off of Cumberland Peninsula had very high aSIC (86.9%) and a high abundance of *F. oceanica* (19.3%) with a low aSST (2.7°C). It is likely that iceberg-derived meltwater, coupled with glacial runoff were causal for this high abundance.

In the Davis Strait and southern Baffin Bay, the West Greenland Current transports temperate and fresh Atlantic Water northwards along the eastern margin, whilst cold Arctic Water is transported southward along the western margin. The aSIC is very high (88.9%–99.1%), with the exception of one anomalous offshore site in northern Davis Strait which registered no aSIC at all, and the average aSST is relatively low (3.2°C). All of these sites had very low to low

abundances of *F. oceanica* (0.4%–7.2%) and as a specific region, 66°N–72.5°N had the least average abundance of the entire northern North Atlantic (2.7%). Large icebergs (>1 million tons) are conveyed northwards from Disko Bay, however any meltwaters appear to have had a negligible effect upon abundance. The upwelling of relatively warmer and more saline Irminger Current derived waters northwards of 64°N may have been the cause for the very low abundances (Boertmann *et al*. 2013; Krawczyk *et al*. 2016; *Oksman et al*. 2017a).

Northern Baffin Bay is dominated by the influx of cold Arctic Water from The Arctic Ocean via the Nares Strait and James and Lancaster Sound's, with very high aSIC (78.7%–97.8%) and low average aSST (2.8°C) (Tang *et al*. 2004). The combination of currents, winds and physical barrier of the ice bridge result in The North Water Polynya remaining partially ice-free at the mouth of the Nares Strait and James and Lancaster Sound's (Dunbar *et al*. 1969; Tang *et al*. 2004). Corresponding to this area of the North Water Polynya, abundances are moderate to high (11.6%–22.5%). The stratified water column, with a large surficial presence of fresh water in the North Water Polynya may be causal to these elevated abundances. A site just south of the North Water Polynya had a low abundance of *F. oceanica* (5.5%) at very high aSIC (94.4%).

F. oceanica appears to be tolerant of a wide range of environmental conditions; from 10.4% abundance at no aSIC and high aSST (6.6°C) to 29% abundance at very high aSIC (80%) and very low aSST (1.3°C). High abundances (17.6%) corresponding with the very high aSIC (82.2%) in the North Water Polynya are juxtaposed by the very low abundances (2.7%) corresponding with the even higher aSIC (85%) in southern Baffin Bay. Based on previous studies the grouped *F. oceanica* is associated with pack ice and the spring bloom coeval to initial sea-ice melt (Von Quillfeldt, 2000; 2001; Miettinen *et al*. 2015; Oksman *et al*. 2019). This propensity for *F. oceanica* to be present in the MIZ where sea ice is melting appears to also be apparent in nearshore areas where the water column is stratified, with a fresher, colder meltwater layer on the surface. The high abundances near Scoresby Sound (29.4%) and off the Cumberland Peninsula (19.3%) in addition to the high North Water Polynya abundances are indicative of a relationship to fresh meltwater from both sea ice, glacial melt and icebergs. Indeed, the RDA (Figure 9) indicates that *F. oceanica* is a 'cold-mixed' water species related to lower aSIC and cold aSST, analogous to *R. hebetata*. f. *hebetata*. Moreover, the environmental response curve (Figure 11) verifies that *F. oceanica* has a statistically significant relationship to both

cold aSST with highest abundances having an optimum at <4°C, and to aSIC with highest abundances having a bimodal optimum both <30% and >75% aSIC. High abundances of *F. oceanica* are indicative of cold water, sea ice or a surficial meltwater layer in a stratified water column, and thus the species must not be considered on its own, but in conjunction to other species.

The species *F. reginae-jahniae* has previously been described as a high-latitude sea-ice diatom (Jensen, 2003; Krawczyck *et al*. 2014; 2016). Largely this holds true with occurrences north of 74°N in Baffin Bay having moderate abundances (6.9%) and several sites northwards of 78°N in the Fram Strait having similar abundances. The highest abundances in the Greenland Sea (6%–7.2%) occur along the West Fram Strait sea-ice edge, where aSIC are moderate (24.2%–33.8%) and the aSST are dominated by cold Arctic Water (2°C–2.4°C). The Atlantic Water derived warmer waters in the eastern Greenland Sea generally have low abundances of *F. reginae-jahniae* (<3%) with aSIC generally being very low (<2.4%) with the exception of the site in the Hornsund Through which had higher aSIC (32.9%). Further north on the West Spitsbergen Slope abundances are relatively high for the species (4.8%–6.7%) whilst aSIC is very low (0.5%–2.8%). A site with very high aSIC (89.7%) on the Greenland Shelf had low abundances of *F. reginae-jahniae* (3.2%) and warm aSST (4.1°C).

South of 75°N along the Greenland Margin and along the West Fram Strait sea-ice edge the abundances of *F. reginae-jahniae* are very low (<1.2%) whilst aSIC are moderate to high (33.9%–59.5%) and aSST are very low (1.2°C–2°C). The nearshore Scoresby Sound Shelf site yields a higher abundance (5.5%) at very high levels of aSIC (80%). The highest abundances of *F. reginae-jahniae* generally correlate with the Arctic Water dominated areas with higher aSIC, but abundances can also be relatively high in areas where sea-ice concentrations are very low. The meltwater input from the system of fjords appears to have an effect upon the abundance of *F. reginae-jahniae*.

To the west of Greenland in the northern Labrador Sea the abundances of *F. reginae-jahniae* are generally very low (0%–1.1%) at moderate to high aSIC (17.5%–79.9%) and warm Atlantic Water dominated aSST (4.1°C–6.4°C). One site in the southern Davis Strait registered a slightly higher abundance (4.3%). In the cold Baffin Current influenced site off Cumberland Peninsula,

a significantly higher abundance of *F. reginae-jahniae* was registered (14.2%) at very high aSIC (86.9%). This peak in abundance nearshore in cold Arctic Water with very high aSIC is analogous to the peak at the Scoresby Sound Shelf.

In the Davis Strait and southern Baffin Bay the abundances of *F. reginae-jahniae* are consistently low (0.4%–3.3%) at very high aSIC (88.8%–99.1%), but also equivalent at the anomalous site with no aSIC. Two sites that yield the low, but relatively higher abundances (3.1% and 3.3%) are located nearshore Cape Adair and Home Bay in western Baffin Bay. The upwelling of the warmer, saline Irminger Current derived waters may be causal to this lack of abundance.

In northern Baffin Bay, the abundances are consistently relatively high for *F. reginae-jahniae* (4.1%–9.6%) at very high aSIC (78.7%–97.8%), with only the Cumberland Peninsula site yielding a higher abundance. The abundances of the two Lancaster Sound sites (5.7%–8.3%) at very high aSIC (95.9%–97.8%) are analogous to the James Sound site (6.4%) which had very high aSIC (78.7%). The cold aSST at the sites was also very similar (3.3°C–3.4°C). The northern Baffin Bay site had the lowest abundance of the area (4.1%) in very high aSIC (94.4%). The North Water Polynya sites were the most abundant (6.4%–9.6%) at high aSIC (80.2%–84.3%) and cold aSST (2.2°C–2.4°C). The characteristic stratified water column of the region may be conducive to the relatively elevated local abundances.

F. reginae-jahniae is a species that does appear to be common but not very abundant at higher latitudes, in agreement with previous literature (Jensen, 2003; Krawkczyck *et al*. 2014; 2016). The highest average abundances in the North Water Polynya and near Lancaster and Jones Sounds, as well as in the West Fram Strait sea-ice edge are indicative of *F. reginae-jahniae* being primarily a MIZ species, with a proclivity for cold, fresher waters (<3°C) with very high aSIC. Similarly, the lower latitude site off Cumberland Peninsula had the highest abundances (14.2%) in cold aSST (2.7°C) with a very high aSIC (86.9%). These results would appear to validate the suggestion of Limoges *et al*. (2018) that *F. reginae-jahniae* is representative of the cold, low salinity conditions of the MIZ. Indeed, the RDA (Figure 9) indicates that *F. reginae-jahniae* is related to high aSIC and cold aSST, analogous to *P. glacialis* and the original grouped *F. oceanica*. Moreover, the environmental response curve (Figure

12) verifies that *F. reginae-jahniae* has a statistically significant relationship to both cold aSST with highest abundances having an optimum at 3°C, and to aSIC with highest abundance having an optimum at >75% aSIC. The close proximity of the plots of *F. reginae-jahniae* and the grouped *F. oceanica* in the RDA indicates that *F. reginae-jahniae* is characteristic of the grouped *F. oceanica* in Oksman *et al*. (2019) and subsequent citing literature. High abundances of *F. reginae-jahniae* are indicative of the MIZ in an Arctic Water dominated area that experiences significant aSIC.

The species *F. arctica* has been associated with Arctic Waters that are influenced by sea-ice (von Quillfeldt, 2000), appearing early in the spring bloom, before *F. oceanica* (von Quillfeldt, 2001). Similar to both *F. oceanica* and *F. reginae-jahniae*, it is considered to be associated to the cold low salinity conditions of the MIZ (Limoges *et al*. 2018). The abundance of *F. arctica* for the northern North Atlantic is distinctive, with low abundances in the Greenland Sea (0%–4.3%), slightly higher abundances in the Davis Strait (0%–8.9%) and a significant increase to maximum abundances in the North Water Polynya (13.7%–26.4%) (Figure 8). The abundances in the Greenland Sea north of 75°N are uniformly very low. One site in the West Spitsbergen Slope had a minor increase in abundance (4.3%) at very low aSIC (2.8%) and warm aSST (4.4°C). Excluding this site, the abundances were low regardless of the environmental variables – with no *F. arctica* present at a Fram Strait site with no aSIC, and very low abundance (0.4%) in the Greenland Shelf site with very high aSIC (89.7%). The unstratified waters of this high aSIC site may also be a factor in the low abundance. The relatively warm waters of the eastern Greenland Sea are evidently not preferential for *F. arctica*. The colder aSST (1.9°C–2.5°C) East Greenland Current sites at the West Fram Strait ice edge and the Greenland Basin all had relatively low to moderate aSIC (2.9%–33.8%). Potentially these low aSIC conditions may be causal to the low abundances seen in the western Greenland Sea.

South of 75°N along the East Greenland margin the abundances of *F. arctica* remain low (0.6%–2.6%) at a moderate to high aSIC (33.9%–59.5%) and cold aSST (1.2°C–2°C). The Scoresby Sound Shelf site had a slightly higher abundance (3.8%) at very high aSIC (80%) and cold aSST (1.3°C). Similar to both *F. oceanica* and *F. reginae-jahniae*, the relatively elevated abundance of *F. arctica* at this nearshore site, indicates that fresh meltwater outflow from the system of fjords is conducive to higher abundances.

To the west of Greenland, in the relatively warm northern Labrador Sea and southernmost Davis Strait (4.6°C–6.4°C), the abundances of *F. arctica* were very low (0%–1.1%) whilst the aSIC is moderate to high (17.5%–79.9%). The Baffin Current dominated nearshore site off Cumberland Peninsula had higher abundances (6.3%) in cold aSST (2.7°C) with very high aSIC (86.9%). This nearshore relative increase in abundance in an Arctic Water dominated area is analogous to the Scoresby Sound Shelf site.

In the Davis Strait and southern Baffin Bay, the abundances were very low (0%–2.4%) in both the sites with very high aSIC (88.9%–99.1%) and also the anomalous site with no aSIC. The nearshore site in Home Bay was exceptional, with a moderate abundance (8.9%), in otherwise unremarkable cold aSST (3°C) and very high aSIC (91.3%) conditions. The upwelling warm and saline Irminger Current derived waters appear to be unaccommodating for *F. arctica*.

In northern Baffin Bay, the abundances are consistently high for *F. arctica* (13.4%–26.4%) in cold aSST (2.2°C–3.4°C) with the exception of one anomalous low abundance site (1.8%). The two Lancaster Sound sites had high abundances (24.1%–25.2%) at very high aSIC (95.9%–97.8%). The James Sound site had slightly lower, but still significant abundances (16.8%) at high aSIC (78.7%). The North Water Polynya had high abundances of *F. arctica* (13.7%–26.4%) at high aSIC (80.2%–84.3%). This significant increase in abundance indicates that these polynya conditions and associated Arctic Water have a predilection for *F. arctica*.

In agreement with previous literature (e.g. von Quillfeldt, 2000; Limoges *et al*. 2018), *F. arctica* is a species that favours Arctic Waters with high levels of sea-ice and low salinity in the MIZ. The highest abundances were located in the cold Arctic Water of the North Water Polynya and local northernmost Baffin Bay sites. Abundances were broadly very low for the rest of the northern North Atlantic, except for the Baffin Current dominated nearshore sites at Cumberland Peninsula (6.8%) and Home Bay (8.9%); possibly due to fresher surface waters derived from glacial meltwater. The anomalously low abundances in the Davis Strait and southern Baffin Bay in cold aSST (2.8°C–4°C) and very high aSIC (88.9%–99.1%) was unanimous for *F. arctica*, *F. oceanica* and *F. reginae-jahniae*. The upwelling saline Irminger Current derived waters may affect all three species, and thus salinity should be an

environmental variable that is considered in future studies. They appear to have an association to stratified water columns, so potentially these waters are relatively unstratified.

The relative abundances of the four (>2 µm) protist groups: diatoms, flagellates, dinoflagellates and unidentified cells in Baffin Bay and the Labrador Sea were analysed in Tremblay *et al*. (2014). Diatoms constituted ~50% of the relative abundance in northernmost Baffin Bay and almost ~75% in western Baffin Bay, but less than ~5% in the Davis Strait, southern Baffin Bay and the northern Labrador Sea (Tremblay *et al*. 2014). This corresponds with the relatively high abundances of all three species in the North Water Polynya, Cumberland Peninsula and Home Bay sites. It also corresponds with the low abundances in the Davis Strait, southern Baffin Bay and the northern Labrador Sea. It appears that the other protists may potentially be better sea-ice proxies in these areas of low diatom abundance.

The RDA (Figure 9) indicates that *F. arctica* is a sea-ice species related to very high aSIC and cold aSST, analogous to *C. oculus-iridis*. The affinity for high aSIC appears to be stronger than that of *F. reginae-jahniae*. Moreover, the environmental response curve (Figure 13) verifies that *F. arctica* has a statistically significant relationship to both cold aSST with highest abundances having an optimum at 2.6°C, and to aSIC with highest abundances having an optimum at >75% aSIC. High abundances of *F. arctica* appear to be in Arctic Waters with cold aSST and high aSIC, particularly in the North Water Polynya region. Indeed, von Quillfeldt (1997) found that *F. arctica* constituted up to 77.7% of total assemblages from the Northeast Water Polynya, although it was described as '*Fragilaria* sp. 1'. The high abundances of *F. arctica* in both the North Water Polynya and the Northeast Water Polynya (von Quillfeldt, 1997) indicates that *F. arctica* can be considered as a characteristic polynya species. Analysis of diatom assemblages from other polynya environments could further verify this finding. In addition to high aSIC and low aSST conditions the upwelling of the nutrient rich West Greenland Current in the North Water Polynya (Melling *et al*. 2001), coupled with the early season productivity that the ice-free area affords (Christie & Sommerkorn, 2012; Meltofte *et al*. 2013), may be conducive to the enhanced abundances of *F. arctica*.

The chrysophyte cysts *Archaeomonas* sp. is a species that is described in the land-fast ice and platelet ice off of Antarctica and shown to be present in diverse marine conditions,

particularly around sea-ice break up (Riaux-Gobin & Stumm, 2006). They have been described in Arctic cores from the Late Cretaceous onwards (Dell'Agnese & Clark, 1994; Stickley *et al*. 2008), but are usually not counted in modern Arctic surface-sediment cores. The abundance of *Archaeomonas* sp. is relatively high across the whole of the northern North Atlantic averaging 9.9% in the Greenland Sea and 13.5% in Baffin Bay. In the Atlantic Water dominated eastern Greenland Sea, the abundances of *Archaeomonas* sp. are quite high (7.1%–19.3%) at very low aSIC (0%–2.8%) and warm aSST (3.8°C–6.6°C). The East Spitsbergen Current dominated site at Hornsund Through has a lower abundance (5%) at moderate aSIC (32.9%). In the northern Fram Strait, two cold sea surface temperature sites (2.7°C–3.5°C) yielded equivalent abundances (5.7%–15.6%) at low aSIC (1.7–10.7%). The higher abundance was registered at the warmer aSST (3.5°C) and lower aSIC (1.7%) site. In the West Fram Strait sea-ice edge, the cold Arctic Water dominated sites (1.9°C–2.4°C) had relatively low abundances (5.1%–10.3%) at moderate aSIC (15.2%–33.8%). The very high aSIC site (89.7%) had a low abundance (3.2%). At low aSIC (1.9%–11.7%) in the Greenland Basin, the abundances were high (16.7%–23%) in cold Arctic Water aSST (1.9°C–2.5°C). For the northern Greenland Sea, it is apparent that the highest abundances of *Archaeomonas* sp. (15.9%–23%) occur at very low aSIC (0%–2.8%), but a wide range of aSST (2.5°C–6.6°C).

South of 75°N along the East Greenland Margin and West Fram Strait sea-ice edge, the abundances of *Archaeomonas* sp. are analogous to the West Fram Strait sea-ice edge sites to the north, with moderate abundances (7.2%–10.9%) at moderate to high aSIC (33.9%–59.5%) and cold aSST (1.2°C–2°C). The Scoresby Sound Shelf site had a similar abundance (10.9%) at high aSIC (80%) and low aSST (1.3%). Dissimilar to the northern Greenland Sea region, the southwestern region abundances appear to be consistent at a low aSST (1.2°C–2°C) independent of aSIC.

To the west of Greenland, in the northern Labrador Sea and southernmost Davis Strait the average abundance is low to moderate (1.5%–8.5%). The Atlantic Water dominated sites (4.1°C–6.4°C) are consistently similar in their low relative abundance (3.5%–8.5%) at moderate to high aSIC (17.5%–79.9%), whilst the very low aSIC (0.9%) had a very low abundance (1.5%). The Baffin Current dominated nearshore site off Cumberland Peninsula had an analogous moderate abundance (6.2%) at very high aSIC (86.9%) and cold aSST (2.7°C).

In the Davis Strait and southern Baffin Bay, the abundances vary from moderate to very high (5.5%–42.7%) in very high aSIC (88.9%–99.1%) and low to temperate aSST (2.8°C–4°C). The lowest abundances (5.5%–7.9%) occur in the central Davis Strait at very high aSIC (88.9%–95.9%). In Central Baffin Bay the higher abundances (15.5%–16.8%) occur at very high aSIC (97.7%–99.1%). The highest abundances (23.9%–42.7%) occur in western Baffin Bay and Davis Strait at very high aSIC (91.3%–98.9%). In the central western Davis Strait, the anomalous site with no aSIC also had a very high abundance (30.3%). These high aSIC conditions had relatively low abundances of the diatom species and therefore perhaps indicate that unstratified water conditions prevail here, favourable to *Archaeomonas* sp. Moreover, Tremblay *et al*. (2014) found that unidentified cells constitute up to ~40% of the (>2 µm) protist assemblage in southern Baffin Bay, so perhaps the conditions are propitious to chrysophytes and not diatoms.

In northern Baffin Bay, the abundances of *Archaeomonas* sp. are moderate to high (5.8%–14.4%) at high to very high aSIC (78.7%–97.8%) and cold aSST (2.2°C–3.4°C). The two Lancaster Sound sites had moderate abundances (6.7%–8.5%) at very high aSIC (95.9%–97.8%). The James Sound site had comparable moderate abundances (6.4%) at high aSIC (78.7%). The North Water Polynya sites were the most varied (5.8%–14.4%) at high aSIC (80.2%–84.3%) and cold aSST (2.2°C–2.4°C). The northern Baffin Bay site had a comparable moderate abundance (7.3%) at very high aSIC (94.4%). The abundances in the high to very high aSIC and strong Arctic Water were high, but generally lower than they were in southern Baffin Bay, where the aSST were fractionally warmer due to the upwelling Irminger Current derived waters.

The chrysophyte cysts *Archaeomonas* sp. are certainly abundant in the diverse sea-ice environments of the northern North Atlantic in addition to the Antarctic marine environment (Riaux-Gobin & Stumm, 2006). The highest abundances are found in the very high aSIC (91.3%–98.9%) of western Baffin Bay (23.9%) and western Davis Strait (42.7%), as well as the central western Davis Strait site (30.3%) which had no aSIC. The highest abundances in the Greenland Sea were in the Greenland Basin (23%), in the Fram Strait (19.3%) and in the West Spitsbergen Slope (18.2%) at very low aSIC (0%–2.8%). The abundances are generally quite

high in all of the conditions of the northern North Atlantic, from no aSIC to very high aSIC, and from cold Arctic Water aSST (1.3°C) to warm Atlantic Water aSST (6.6°C). *Archaeomonas* sp. does have high abundances in high aSIC, but its ecology does not appear to be associated just to aSIC. Indeed, the RDA (Figure 9) indicates that *Archaeomonas* sp. is a 'cold mixed' water species related to low aSIC and to cold aSST, analogous to the separated *F. oceanica* and *R. hebetata.* f. *hebetata*. Moreover, the environmental response curve (Figure 14) verifies that *Archaeomonas* sp. has a statistically significant relationship to both aSST with highest abundances having a bimodal optimum at 3.1°C and 6.6°C, and to aSIC with highest abundances having a bimodal optimum at both no aSIC and >75% aSIC. The polarity in highest abundances from the MIZ associated diatom species indicates that *Archaeomonas* sp. is associated with an unstratified water column which has a relatively high salinity. High abundances of *Archaeomonas* sp. may be indicative of either high aSIC, or open water conditions, and thus must not be considered on their own, but in conjunction to other species.

5.2. Recounting of core MD99-2322 on the Southeast Greenland Shelf

The core MD99-2322 from the Kangerlussuaq Trough was measured for the Late Holocene, comprising the last ~2900 years in Miettinen *et al*. (2015). The section of the original core used in this study (Figure 15) constitutes the cold period (~690–1000 CE), the warmer Medieval Climate Anomaly (~1000–1200 CE) and the majority of the colder Little Ice Age (~1200 –1890 CE) (Miettinen *et al*. 2015). The highest abundances of *F. oceanica* occur (>20%) in the cold period (~690–994 CE), when aSIC were relatively high (>40%). The transition to the warmer Medieval Climate Anomaly (~1013–1188 CE), where aSIC fell (<40%), is coeval to a decrease in the abundance of *F. oceanica* to a moderate abundance (~10%). A decrease in aSIC (>40%) concurrent to an aSST peak (6.6°C) ~1100 CE, yields an increase in *F. oceanica* abundance (~20%) at ~1116 CE. This moderate abundance of *F. oceanica* (~10%) during the Medieval Warm period is ascribed to the increased melting of first year ice, which formed on the fresh surficial waters generated from the enhanced melting of glaciers on Greenland (Miettinen *et al*. 2015). During the subsequent cooling at the onset of the Little Ice Age (~1215–1890 CE) aSIC increased (>50%), however *F. oceanica* abundances decreased and stayed continuously low (~5%). This low abundance is attributed to thicker multiyear sea-ice, with much less melting and a significantly decreased MIZ (Miettinen *et al*. 2015).

The grouped *F. oceanica* was separated (Figure 16) to see if the new ecological data from *F. reginae-jahniae, F. arctica* and the chrysophyte cysts *Archaeomonas* sp. would refine the interpretation of the variation in aSIC and contemporaneous changes in abundance. The abundances of both *F. reginae-jahniae* and *F. arctica* were very low throughout the core. The highest abundances (3% and 1.7% respectively) occurred in the cold period (~690–994 CE) synchronous to the highest abundance of *F. oceanica* (26%) and high aSIC (~60%) and lowest aSST (~5°C). During the Medieval Warm Period the abundances decreased in response to the declining aSIC (<40%) and warming aSST (~6°C). *F. reginae-jahniae* remained consistently unabundant (<1%), with an increase (1.7%) occurring (~1116 CE) subsequent to the decrease in aSIC at ~1000 CE, and comparable to the increase in *F. oceanica* abundance from moderate (>10%) to high (17.5%). *F. arctica* remained consistently unabundant (<1%), with a short sharp increase (1.6%) at ~1188 CE before the onset of the Little Ice age, where it decreased again. During the Little Ice Age, the abundance of *F. oceanica* decreased and remained moderate (<6.8%) whilst aSIC increased (>50%) and aSST cooled slightly (5.4°C). The abundance of *F. reginae-jahniae* remained low (<1.1%) throughout the Little Ice Age, with an ephemeral increase (3.2%) at ~1350 CE. Abundances of *F. reginae-jahniae* also remained relatively low throughout the Little Ice Age in the antiphase relationship affected Disko Bay, with two peaks occurring when there were ephemeral increases in aSIC (Seidenkrantz *et al*. 2007; Miettinen *et al*. 2015; Krawczyk *et al*. 2016). The abundance of *F. arctica* remained low (<0.95) throughout the Little Ice Age. The findings of this study indicate that all of the diatom species are associated with a stratified water column. This suggests that the decrease in abundance for *F. oceanica* during the Little Ice Age due to a decreased MIZ, as hypothesised in Miettinen *et al*. (2015) is reasonable and also applicable to both *F. reginae-jahniae* and *F. arctica*. However, due to such low abundances, the variance in *F. reginae-jahniae* and *F. arctica* is not very significant.

The chrysophyte cyst *Archaeomonas* sp. had a relatively high abundance throughout the core (3.2%–16.8%) (Figure 16). Throughout the cold period (~690–994 CE) the abundances of *Archaeomonas* sp. were moderate (5.7%–8.9%) at relatively high aSIC (>40%) and the coldest aSST (~5°C). During the Medieval Climate Anomaly (~1013–1188 CE) abundances increased (12%–13.7%) during a period of relatively high aSIC (~1031–1073 CE) and warmer aSST (~6°C).

Abundances then decreased (5.5%) in response to the decreasing aSIC and cooling aSST. Abundances increased and remained relatively high (10.5%–16.8%) throughout the Little Ice Age (~1214 CE–1498 CE), in response to increasing aSIC (>50%) and cooler aSST (~5.4C.). The highest abundances of *Archaeomonas* sp. occurred in the increased aSIC in the Little Ice Age and in the short period of increased aSIC during the Medieval Warm Period. The increased abundance during these periods of relatively unstratified waters, as evidenced by the low abundances of *F. oceanica*, indicates that *Archaeomonas* sp. has an affinity for these relatively more saline conditions.

The very low abundances of *F. arctica* and *F. reginae-jahniae* throughout the core, particularly in relation to *F. oceanica,* render their separation from the grouped *F. oceanica* inconsequential. Both *F. arctica* and *F. reginae-jahniae* yield their highest abundances at high aSIC and the coldest aSST. The effect of the Irminger Current upon the Kangerlussuaq Trough region is evident, with the warm aSST (>5°C) and moderate to high aSIC (30%–60%) proving to suppress the abundances of these two species. A site from the North Water Polynya, or off the Cumberland Peninsula where both species are certainly more abundant may have yielded more significant results. Nonetheless, this finding indicates that in regions of low abundance for both *F. arctica* and *F. reginae-jahniae,* if they have been grouped under *F. oceanica* in previous literature*,* this should not significantly affect the conclusions. The abundance of *F. oceanica* was largely unaffected by the separation, as it constituted such a significant proportion of the grouped abundances on average (83%).

The relatively high abundance of *Archaeomonas* sp. throughout the core is indicative of their relatively broad ecology (Figure 14). The warmer water in the Kangerlussuaq Trough is ostensibly more accommodating for *Archaeomonas* sp. than either *F. arctica* or *F. reginae-jahniae*, as it yields high abundances in other sites with relatively warmer water, such as in the eastern Fram Strait. The abundance of *Archaeomonas* sp. at both high aSIC and no aSIC is perplexing for trying to reconstruct sea-ice concentrations; however, it does not appear to be strongly associated with the MIZ or a stratified water column. Thus, counting *Archaeomonas* sp. in conjunction with other methods, such as ice rafted detritus (quartz weight %), as Miettinen *et al*. (2015) did for *F. oceanica* abundances is essential.

5.3. Implications for qualitative and quantitative reconstruction

One of the aims of the separation of *F. oceanica* from the training set Miettinen *et al*. (2015) was to improve the diatom-based transfer function for reconstructions of aSST and aSIC. The ecological findings of the separated species will have an implication upon the use of future transfer functions in reconstructing palaeoceanographic and palaeoclimatological conditions. The separation of the species allows for a more nuanced and accurate qualitative interpretation of assemblages, and, as there are evidently subtle differences in their ecologies, these can have an influence on quantitative reconstruction via differences in their SST and SIC optima. High abundances of *F. oceanica* can be interpreted as indicative of melting sea ice, or a cold stratified water column with a fresh surface water component. High abundances of *F. reginae-jahniae* can be interpreted as indicative of the MIZ in a cold aSST low salinity area, with significant aSIC. High abundances of *F. arctica* can be interpreted as indicative of the MIZ in a cold aSST low salinity area, with narrowly defined optima around low SST and very high SIC. Furthermore, very high abundances of *F. arctica* in the North Water Polynya relative to the rest of the northern North Atlantic indicates that the species is intrinsically linked to polynya regions and can thus be regarded as a potential characteristic polynya species. Other studies from other Northern Hemisphere polynya regions are needed to confirm this finding. High abundances of the chrysophyte cyst *Archaeomonas* sp. are common throughout the northern North Atlantic, in a broad range of environmental conditions – from no aSIC to very high aSIC; and cold Arctic Water aSST to warm Atlantic Water aSST. The highest abundances tend to be in non MIZ conditions indicating that *Archaeomonas* sp. favour these relatively more saline conditions. High abundances have to be considered in conjunction to other species or palaeoclimatic proxies.

In areas where abundances of the *F. arctica* and *F. reginae-jahniae* are high, it is crucial for the application of transfer functions that they are separated from *F. oceanica*. It is very likely that interpretations of the severity of aSIC will be elucidated from their abundances or lack thereof. They are also very good indicators of cold aSST, particularly of an Arctic Water signal. Salinity also appears to be very significant for both species as they tend to be most abundant in areas replete with a stratified meltwater surface layer. In areas of low abundances, the

separation may not generate too much novel information, such as in the Kangerlussuaq Trough site, however it is nonetheless important to be able to interpret what the lack of the species may indicate (e.g. a strong Atlantic Water component or unstratified water column). Sites from the North Water Polynya, off Cumberland Peninsula and the Northeast Water Polynya would be the most interesting to analyse downcore with the improved transfer function and species ecological interpretation.

6. CONCLUSIONS

The separated diatoms and chrysophtye cyst *Archaeomonas* sp. exhibited different relationships to the environmental variables aSIC and aSST than the grouped *F. oceanica* species complex from Miettinen *et al*. (2015), verifying the main hypothesis. The separated species *F. oceanica* is a 'cold-mixed' water species with a broad optimum for both cold aSST (<4°C) and both low aSIC (<30%) and high aSIC (>75%). High abundances occur in the MIZ where surficial meltwater is high in the spring bloom, particularly from glacial meltwaters nearshore. *F. reginae-jahniae* is a sea-ice species related to cold aSST (3°C) and high aSIC (>75%). High abundances occur in the low salinity Arctic Water dominated MIZ which experiences significant aSIC. *F. arctica* is a sea-ice species related to cold aSST (2.6°C) and high aSIC (>75%). High abundances occur in the low salinity Arctic Water dominated MIZ which experiences severe aSIC, particularly in polynya conditions that are influenced by nutrient upwelling and early season productivity. *F. arctica* can be considered a characteristic polynya species at high abundances. The chrysophyte cyst *Archaeomonas* sp. is a 'cold-mixed' water species bimodally related to cold aSST and aSIC. High abundances occur in both warm ice-free Atlantic Water and high aSIC Arctic Water conditions resulting in *Archaeomonas* sp. being a more complex indicator for aSST or aSIC, potentially similar to *F. cylindrus* in Oksman *et al*. (2019). However, the aversion to MIZ conditions indicates that the species has an affinity to relatively saline unstratified water columns, potentially verifying the second hypothesis. This is the first time that the distribution and ecology of *Archaeomonas* sp. has been presented. As such, the ecology described here can be used in future studies. The separation of the three diatom species is crucial for the ecological interpretation of downcore assemblage changes. It is also crucial for the application of transfer functions in order to have greater precision in reconstructing aSIC and assessing the influence of Arctic Water or Atlantic Water, even at low abundances.

7. ACKNOWLEDGEMENTS

I would like to thank my supervisors Maija Heikkilä, Kaarina Weckström and Heikki Seppä for all of their support, patience and wisdom over the past year. Maija, thank you for inviting me to join the project as a research assistant. Kaarina, thank you for both teaching me how to recognise the species and offering so many hours of your time towards the analysis. Thanks to Arto Miettinen for allowing me to reanalyse the training set, the Kangerlussuaq Trough site core and answering my questions. Thanks to Stephen Juggins for helping with the analysis and particularly with the environmental response curves. Special mention to my partner Olivia who has endured a lot of diatom-centric discussion.

8. REFERENCES

Aagaard, K. & Coachman, L. K. 1968a. The East Greenland Current north of Denmark Strait, Part I. *Arctic*, 21, 181-200.

Alley, R., Mayewski, P., Sowers, T., Stuiver, M., Taylor, K. & Clark, P. 1997. Holocene climatic instability: A prominent, widespread event 8200 yr ago. Geology, 25(6), 483-486.

AMAP, 2017. Snow, water, ice and permafrost in the Arctic (SWIPA) 2017. Arctic Monitoring and Assessment Programme (AMAP), Oslo, Norway. XIV, 269pp.

Andersen, C., Koç, N., Jennings., A. & Andrews, J. T. 2004a. Nonuniform response of the major surface currents in the Nordic Seas to insolation forcing: implications for the Holocene climate variability. Paleoceanography, 19(2), PA2003.

Andersen, C., Koç, N. & Moros, M. 2004b. A highly unstable Holocene climate in the subpolar North Atlantic: Evidence from diatoms. Quaternary Science Reviews, 23(20), 2155-2166.

Bartoli, G., Sarnthein, M., Weinelt, M., Erlenkeuser, H., Garbe-Schönberg, D. & Lea, D. W. 2005. Final closure of Panama and the onset of Northern Hemisphere Glaciation. Earth and Planetary Science Letters*,* 237(1-2), 33-44.

Belt, S. T., Massé, G., Rowland, S. J., Poulin, M., Michel, C. & LeBlanc, B. 2007. A novel chemical fossil of palaeo sea-ice: IP25. Organic Geochemistry, 38(1), 16-27.

Belt, S. T. & Müller, J. 2013. The Arctic sea-ice biomarker IP25: A review of current understanding, recommendations for future research and applications in palaeo sea-ice reconstructions. Quaternary Science Reviews, 79, 9-25.

Berner, K. S., Koç, N., Divine, D., Godtliebsen, F. & Moros, M. 2008. A decadal-scale Holocene sea surface temperature record from the subpolar North Atlantic constructed using diatoms and statistics and its relation to other climate parameters. Paleoceanography, 23(2), PA2210.

Birks, H. J. B. & Koç, N. 2002. A high-resolution diatom record of Late-Quaternary sea-surface temperatures and oceanographic conditions from the eastern Norwegian Sea. Boreas, 31(1), 323-344.

Boertmann, D., Mosbech, A., Schiedek, D. & Dünweber, M. 2013. Disko West: A strategic environmental impact assessment of hydrocarbon activities. Aarhus University, DCE – Danish Centre for Environment and Energy, 71, 306pp. Scientific Report from DCE – Danish Centre for Environment and Energy No. 71.

Broecker, W. 2006. Was the Younger Dryas Triggered by a Flood? Science, 312(5777), 1146-1148.

Brown, T. & Belt, S. T. 2017. Biomarker-based H-print quantifies the composition of mixed sympagic and pelagic algae consumed by Artemia sp. Journal of Experimental Marine Biology and Ecology, 488, 32-37.

Budikova, D. 2009. Role of Arctic sea ice in global atmospheric circulation: a review. Global and Planetary Change, 68(3), 149-163.

Calvert, S. E. & Pedersen, T. F. 2007. Chapter fourteen elemental proxies for palaeoclimatic and palaeoceanographic variability in marine sediments: interpretation and application. Developments in marine geology. Elsevier Science & Technology, 567-644pp.

Carlson, A. E. 2013. The Younger Dryas climate event. Encyclopedia of quaternary science, 3. Elsevier, Amsterdam, 126-134pp.

Christie, P. & Sommerkorn, M. 2012. RACER: Rapid assessment of circum-Arctic ecosystem resilience, 2nd ed. Ottawa, Canada: WWF Global Arctic Program, 72pp.

Crutzen, P. J. & Stoermer, E. F. 2000. *IGBP* Newsletter, 41. Royal Swedish Academy of Sciences, Stockholm.

Curry, J. A., Schramm, J. L. & Ebert, E. E. 1995. Sea-ice–Albedo climate feedback mechanism. Journal of Climate, 8(2), 240-247.

Dell'Agnese, D. J. & Clark, D. L. 1994. Siliceous microfossils from the warm Late Cretaceous and Early Cenozoic Arctic Ocean. Journal of Paleontology, 68(1), 31-47.

De Sève, M. A. 1999. Transfer function between surface sediment diatom assemblages and sea surface temperature and salinity of the Labrador Sea. Marine Micropaleontology, 36(4), 249-267.
De Vernal, A., Gersonde, R., Goosse, H., Seidenkrantz, M. & Wolff, E. W. 2013. Sea ice in the paleoclimate system: the challenge of reconstructing sea ice from proxies – an introduction. Quaternary Science Reviews, 79, 1-8.
Dickson, B. & Brown, J. 1994. The production of North Atlantic deep water: Sources, rates, and pathways. Journal of Geophysical Research - Oceans, 99(C6), 12319-12341.
Dickson, B., Yashayaev, I., Meincke, J., Holfort, J., Turrell, B., Dye, S. &. Holfort, J 2002. Rapid freshening of the deep North Atlantic Ocean over the past four decades. Nature, 416(6883), 832-837.
Dickson, B., Dye, S., Jónsson, S., Köhl, A., Macrander, A., Marnela, M., Meincke, J., Olsen, S., Rudels, B., Valdimarsson, H. & Voet, G. 2008. The overflow flux west of Iceland: Variability, origins and forcing. In: Dickson, R. R., Meincke, J. & Rhines, P. (Eds.) Arctic–Subarctic ocean fluxes. Springer, Dordecht, 443-474.
Digby, P. S. B. 1953. Plankton production in Scoresby Sound, East Greenland. Journal of Animal Ecology, 22(2), 289-322.
Divine, D. V. & Dick, C. 2006. Historical variability of sea ice edge position in the Nordic Seas. Journal of Geophysical Research - Oceans, 111(C1), C01001.
Dunbar, M. 1969. The geographical position of the North Water. Arctic, 22(4), 438-441.
Ehlers, J., Gibbard, P. L., Hughes, P. D., Gibbard, P. L. & Hughes, P. D. 2011. Quaternary glaciations - extent and chronology: A closer look. Elsevier, Amsterdam, 1126pp.
Fahrbach, E., Meincke, J., Osterhus, S., Rohardt, G., Schauer, U., Tverberg, V. & Verduin, J. 2001. Direct measurements of volume transport through Fram Strait. *Polar Research,* 20, 217-224.
Fetterer, F., Knowles, K., Meier, W. & Savoie, M. 2018. Updated Daily. Sea ice index, version 2.1. Arctic monthly median extent. Boulder Colorado USA. NSIDC: National Snow and Ice Data Center. Accessed 8th November 2018. https://nsidc.org/
Fischer, J., Karstensen, J., Zantopp, R., Visbeck, M., Biastoch, A., Behrens, E., Böning, C. W., Quadfasel, D., Jochumsen, K., Valdimarsson, H., Jónsson, S., Bacon, S., Holliday, N. P., Dye, S., Rhein, M. & Mertens, C. 2015. Intra-seasonal variability of the DWBC in the western subpolar North Atlantic. Progress in Oceanography, 132, 233-249.
Fratantoni, P. S. & Pickart, R. S. 2007. The western North Atlantic shelfbreak current system in summer. Journal of Physical Oceanography, 37(10), 2509-2533.
Funck, T., Gohl, K., Damm, V. & Heyde, I. 2012. Tectonic evolution of southern Baffin Bay and Davis Strait: Results from a seismic refraction transect between Canada and Greenland. Journal of Geophysical Research, 117(4), B04107.
Gersonde, R. & Harwood, D. M. 1990. Proceeding of the Ocean Drilling Program, Scientific Results, 113(1), 365-402.
Hakkinen, S. & Rhines, P. B. 2009. Shifting surface currents in the northern North Atlantic Ocean. Journal of Geophysical Research - Oceans, 114(C4), C04005.
Hasle, G. R., Syvertsen, E. E. & von Quillfeldt, C. H. 1996. *Fossula arctica* gen. nov. spec. nov., a marine Arctic araphid diatom. Diatom Research, 11, 261-272.
Haugan, P. M. 1999. Structure and heat content of the West Spitsbergen Current. Polar Research, 18(2), 183-188.
Haywood, A. M., Dowsett, H. J. & Dolan, A. M. (2016). Integrating geological archives and climate models for the Mid-Pliocene Warm Period. Nature Communications, 7(1), 10646.
Hegerl, G. C. & Bindoff, N. L. 2005. Warming the world's oceans. Science, 309(5732), 254-255.
Heikkilä, M. & Seppä, H. 2010. Holocene climate dynamics in Latvia, eastern Baltic region: A pollen-based summer temperature reconstruction and regional comparison. Boreas, 39(4), 705-719.
Hoffman, J., Carlson, A., Winsor, K., Klinkhammer, G., LeGrande, A., Andrews, J. & Strasser, J. 2012. Linking the 8.2 Ka Event and its freshwater forcing in the Labrador Sea. Geophysical Research Letters, 39(18).
Imbrie, J. & Imbrie, K. P. (1986). Ice Ages: Solving the Mystery. Harvard University Press, 158pp.

IPCC, 2001. In: Houghton, J. T., Ding, Y., Griggs, D. J., Noguer, M., van der Linden, P. J., Dai, X., Maskell, K., & Johnson, C. A. 2003. IPCC, 2001. climate change 2001: The scientific basis. contribution of working group 1 to the third assessment report of the intergovernmental panel on climate change. International Journal of Epidemiology*, 32*(2), 321pp.

IPCC, 2018: Masson-Delmotte, V., Zhai, P., Pörtner, H. O., Roberts, D., Skea, J., Shukla, P. R., Pirani, A., Moufouma-Okia, W., Péan, C., Pidcock, R., Connors, S., Matthews, J. B. R., Chen, Y., Zhou, X., Gomis, M. I., Lonnoy, E., Maycock, T., Tignor, M. & Waterfield, T. (Eds.) Summary for Policymakers. In: Global warming of 1.5°C. An IPCC Special Report on the impacts of global warming of 1.5°C above pre-industrial levels and related global greenhouse gas emission pathways, in the context of strengthening the global response to the threat of climate change, sustainable development, and efforts to eradicate poverty. World Meteorological Organization, Geneva, Switzerland, 32 pp.

Jakobsson, M., Mayer, L., Coakley, B., Dowdeswell, J. A., Forbes, S., Bridman, B., Hodnesdal, H., Noormets, R., Pedersen, R., Rebesco, M., Schenke, H. W., Zarayskaya, Y., Accettella, D., Armstrong, A., Anderson, R. M., Bienhoff, P., Camerlenghi, A., Church, I., Edwards, M., Gardner, J. V., Hall, J. K., Hell, B., Hestvik, O., Kristoffersen, Y., Marcussen, C., Mohammed, R., Mosher, D., Nghiem, S. V., Pedrosa, M. T., Travaglin, P. G. & Weatherall, P. 2012. The international bathymetric chart of the Arctic Ocean (IBCAO) version 3.0. Geophysical Research Letters Vol. 39*,* L12609, 1-6.

Jansen, F. & Oksanen, J. 2013. How to model species responses along ecological gradients – Huisman-Olff-Fresco models revisited. Journal of Vegetation Science, 24, 1108-1117.

Jensen, K. G. 2003. Holocene hydrographic changes in Greenland coastal waters. the Geological Survey of Denmark and Greenland, Denmark, 160pp. (PhD Thesis).

Ji, R., Jin, M. & Varpe, Ø. 2013. Sea ice phenology and timing of primary production pulses in the Arctic Ocean. Global Change Biology, 19(3), 734-741.

Jiang, H., Seidenkrantz, M., Knudsen, K. L. & Eiríksson, J. 2001. Diatom surface sediment assemblages around Iceland and their relationships to oceanic environmental variables. Marine Micropaleontology, 41(1), 73-96.

Jiang, H., Seidenkrantz, M., Knudsen, K. L. & Eiríksson, J. 2002. Late-Holocene summer sea-surface temperatures based on a diatom record from the North Icelandic shelf. The Holocene, 12(2), 137-147.

Jiang, H., Eiriksson, J., Schulz, M., Knudsen, K. & Seidenkrantz, M. 2005. Evidence for solar forcing of sea-surface temperature on the North Icelandic Shelf during the Late Holocene. Geology, 33(1), 73-76.

Jiang, H., Muscheler, R., Björck, S., Seidenkrantz, M., Olsen, J., Sha, L., Sjolte, J., Eiríksson, J., Ran, L., Knudsen, K. L. & Knudsen, M. F. 2015. Solar forcing of holocene summer sea-surface temperatures in the northern north atlantic. *Geology, 43*(3), 203-206. doi:10.1130/G36377.1

Jochumsen, K., Quadfasel, D., Valdimarsson, H. & Jónsson, S. 2012. Variability of the Denmark Strait overflow: moored time series from 1996–2011. Journal of Geophysical Research, 117, C1203.

Jochumsen, K., Köllner, M., Quadfasel, D., Dye, S., Rudels, B. & Valdimarsson, H. 2015. On the origin and propagation of Denmark Strait overflow water anomalies in the Irminger Basin. Journal of Geophysical Research: Oceans, 120(3), 1841-1855.

Jordan, R. W. & Stickley, C. E. 2010. Diatoms as indicators of paleoceanographic events. In: Smol, J. P. & Stoermer, E. F. (Eds.) The Diatoms: Applications for the Environmental and Earth Sciences, 2nd Edition. Cambridge University Press, 424-453pp.

Juggins, S & Birks, H. J. B. 2012. Quantitative environmental reconstructions from biological data. Tracking environmental change using lake sediments. *Dordrecht: Springer Netherlands.* pp. 431-494.

Juggins. S. 2014. C2 Version 1.7. https://www.staff.ncl.ac.uk/stephen.juggins/software.html

Justwan, A. & Koç, N. 2008. A diatom based transfer function for reconstructing sea ice concentrations in the North Stlantic. Marine Micropaleontology, 66(3), 264-278.

Justwan, A. & Koç, N. 2009. Evolution of the East Greenland Current between 1150 and 1740 AD, revealed by diatom-based sea surface temperature and sea-ice concentration reconstructions. Polar Research, 28(2), 165-176.

Justwan, A., Koç, N. & Jennings, A. E. 2008. Evolution of the Irminger and East Icelandic Current systems through the Holocene, revealed by diatom-based sea surface temperature reconstructions. Quaternary Science Reviews, 27(15), 1571-1582.

Kattsov, V. M., Källén, E., Cattle, H. P., Christensen, J., Drange, H., Hanssen-Bauer, I., Jóhannesen, T., Karol, I., Räisänen, J., Svensson, G. & Vavulin, S. 2005. Future climate change: Modeling and scenarios for the arctic. In: Arctic Climate Impact Assessment. Cambridge University Press, London, 99-150.

Kobashi, T., Severinghaus, J., Brook, E., Barnola, J. & Grachev, A. 2007. Precise timing and characterization of abrupt climate change 8200 years ago from air trapped in polar ice. Quaternary Science Reviews, 26(9-10), pp. 1212-1222.

Koç Karpuz, N. & Schrader, H. 1990. Surface sediment diatom distribution and Holocene paleotemperature variations in the Greenland, Iceland and Norwegian Sea. Paleoceanography, 5(4), 557-580.

Koç, N. & Jansen, E. 1994. Response of the high-latitude northern hemisphere to orbital climate forcing: Evidence from the Nordic Seas. Geology, 22(6), 523-526.

Koç, N., Klitgaard-Kristensen, D., Hasle, K., Forsberg, C. F. & Solheim, A. 2002. Late glacial paleoceanography of Hinlopen Strait, northern Svalbard. Polar Research, 21(2), 307-314.

Koshkarova, V. L. & Koshkarov, A. D. 2004. Regional signatures of changing landscape and climate of northern central Siberia in the Holocene. Russian Geology & Geophysics, 45(6), 672-685.

Krawczyk, D. W., Witkowski, A., Moros, M., Lloyd, J., Kuijpers, A. & Kierzek, A. 2010. Late-Holocene diatom-inferred reconstruction of temperature variations of the West Greenland Current from Disko Bugt, central West Greenland. The Holocene, 20(5), 659-666.

Krawczyk, D. W., Witkowski, A., Lloyd, J., Moros, M., Harff, J. & Kuijpers, A. 2013. Late-Holocene diatom derived seasonal variability in hydrological conditions off Disko Bay, West Greenland. Quaternary Science Reviews, 67, 93-104.

Krawczyk, D. W., Witkowski, A., Waniek, J., Wroniecki, M. & Harff, J. 2014. Description of diatoms from the southwest to west Greenland coastal and open marine waters. Polar Biology, 37(11), 1589-1606.

Krawczyk, D. W., Witkowski, A., Moros, M., Lloyd, J. M., Høyer, J. L., Miettinen, A. & Kuijpers, A. 2016. Quantitative reconstruction of Holocene sea ice and sea surface temperature off West Greenland from the first regional diatom data set. Paleoceanography, 32(1), 18-40.

Leu, E., Mundy, C. J., Assmy, P., Campbell, K., Gabrielsen, T. M., Gosselin, M., Juul-Pedersen, T. & Gradinger, R. 2015. Arctic spring awakening – steering principles behind the phenology of vernal ice algal blooms. Progress in Oceanography, 139, 151-170.

Limoges, A., Masse, G., Weckström, K., Poulin, M., Ellegaard, M., Heikkila, M., Geilfus, N-X., Sejr, M. K., Rysgaard, S. & Ribeiro, S. 2018. Spring succession and vertical export of diatoms and IP25 in a seasonally ice-covered High Arctic fjord. In: Frontiers in Earth Science, 6, 226.

Lisiecki, L. E. & Raymo, M. E. 2005. A Pliocene-Pleistocene stack of 57 globally distributed benthic δ18O records. Paleoceanography, 20(1), PA1003.

Lloyd, J. M., Kuijpers, A., Long, A., Moros, M. & Park, L. A. 2007. Foraminiferal reconstruction of Mid- to Late-Holocene ocean circulation and climate variability in Disko Bugt, West Greenland. The Holocene, 17(8), 1079-1091.

Lundholm, N. & Hasle, G. R. 2010. Fragilariopsis (Bacillariophycaea) of the Northern Hemisphere – morphology, taxonomy, phylogeny and distribution, with a description of F. pacifica sp. nov. Phycologia, 49(5), 438-460.

Mann, M. E., & Jones, P. D. 2003. Global surface temperatures over the past two millennia. Geophysical Research Letters, 30(15).

Mann, M. E., Zhang, Z., Rutherford, S., Bradley, R. S., Hughes, M. K., Shindell, D., Ammann, C., Faluvegi, G. & Ni, F. 2009. Global signatures and dynamical origins of the Little Ice Age and Medieval Climate Anomaly. Science, 326(5957), 1256-1260.

Mauritzen, C. 1996. Production of dense overflow waters feeding the North Atlantic across the Greenland-Scotland Ridge. Part 1: Evidence for a revised circulation scheme. Deep Sea Research Part 1, 43(6), 769-806.

McCartney, M. S. & Mauritzen, C. 2001. On the origin of the warm inflow to the Nordic Seas. Progress in Oceanography, 51(1), 125-214.

Meltofte, H. 2013. Arctic biodiversity assessment: status and trends in Arctic biodiversity. (Eds.) CAFF International Secretariat, 674pp.

Melling, H., Gratton, Y. & Ingram, G. 2001. Ocean circulation within the North Water polynya of Baffin Bay, Atmosphere-Ocean, 39(3), 301-325.

Miettinen, A., Koç, N., Hall, I., Godtliebsen, F. & Divine, D. 2011. North Atlantic sea surface temperatures and their relation to the North Atlantic Oscillation during the last 230 years. Climate Dynamics, 36(3), 533-543.

Miettinen, A., Divine, D., Koç, N., Godtliebsen, F. & Hall, I. R. 2012. Multicentennial variability of the sea surface temperature gradient across the subpolar North Atlantic over the last 2.8 kyr. Journal of Climate, 25(12), 4205-4219.

Miettinen, A., Divine, D. V., Husum, K., Koç, N. & Jennings, A. 2015. Exceptional ocean surface conditions on the SE Greenland Shelf during the Medieval Climate Anomaly. Paleoceanography, 30(12), 1657-1674.

Miettinen, A. 2018. Diatoms in Arctic regions: potential tools to decipher environmental changes. Polar Science, 18, 220-226.

Migoń, P. 2010. Geomorphological landscapes of the world. Dordecht: Springer, Netherlands. 227pp.

Monastersky, R. 2013. Global carbon dioxide levels near worrisome milestone. Nature, 497(7447), 13-14.

Moros, M., Lloyd, J. M., Perner, K., Krawczyk, D., Blanz, T., de Vernal, A., Ouellet-Bernier, M-M., Kuijpers, A., Jennings, A. E., Witkowski, A., Schneider, R. & Jansen, E. 2016. Surface and sub-surface multi-proxy reconstruction of Middle to Late Holocene palaeoceanographic changes in Disko Bugt, West Greenland. Quaternary Science Reviews, 132, 146-160.

Myers, P. G., Donnelly, C. & Ribergaard, M. H. 2009. Structure and variability of the West Greenland Current in summer derived from 6 repeat standard sections. Progress in Oceanography, 80(1), 93-112.

Muschitiello, F. 2016. Deglacial impact of the Scandinavian Ice Sheet on the North Atlantic climate system. Stockholm University, Sweden, 59pp. (PhD Thesis).

Müller, R. D., Sdrolias, M., Gaina, C. & Roest, W. R. 2008. Age, spreading rates, and spreading asymmetry of the world's ocean crust. Geochemistry Geophysics Geosystems, 9(4).

Oksman, M., Weckström, K., Miettinen, A., Juggins, S., Divine, D. V., Jackson, R., Telford, R., Korsgaard, N. & Kucera, M. 2017a. Younger Dryas ice margin retreat triggered by ocean surface warming in central-eastern Baffin Bay. Nature Communications, 8, 1017.

Oksman, M., Weckström, K., Miettinen, A., Ojala, A. E. K. & Salonen, V. P. 2017b. Late Holocene shift towards enhanced oceanic variability in a High-Arctic Svalbard fjord (79°N) at 2500 cal. yr BP. *Arktos, 3*(1), 4.

Oksman, M., Juggins, S., Miettinen, A., Witkowski, A & Weckström, K. 2019. The biogeography and ecology of common diatom species in the northern North Atlantic, and their implications for palaeoceanographic reconstructions. Marine Micropaleontology, 148.

Orvik, K. A. & Niiler, P. 2002. Major pathways of Atlantic Water in the northern North Atlantic and Nordic Seas toward Arctic. Geophysical Research Letters, 29(19), 4.

Orvik, K. A. & Skagseth, Ø. 2005. Heat flux variations in the eastern Norwegian Atlantic Current toward the Arctic from moored instruments, 1995–2005. Geophysical Research Letters, 32(14), L14610.

Pearce, C., Seidenkrantz, M., Kuijpers, A. & Reynisson, N. F. 2014a. A multi-proxy reconstruction of oceanographic conditions around the Younger Dryas–Holocene transition in Placentia Bay, Newfoundland. Marine Micropaleontology, 112, 39-49.

Pearce, C., Weckström, K., Sha, L., Miettinen, A. & Seidenkrantz, M. 2014b. The Holocene marine diatom flora of eastern Newfoundland Bays. Diatom Research, 29(4), 441-454.

Perch-Nielsen, K. 1978. Eocene to Pliocene archaeomonads, ebridians, and endoskeletal dinoflagellates from the Norwegian Sea. DSDP Leg 38, Initial Report Deep Sea Drilling Project, 38(supplement), 147-175.

Pollard, R. T., Read, J. F., Holliday, N. P. & Leach, H. 2004. Water masses and circulation pathways through the Iceland Basin during Vivaldi 1996. Journal of Geophysical Research - Oceans, 109(C4), C04004.

Polyak, L., Alley, R. B., Andrews, J. T., Brigham-Grette, J., Cronin, T. M., Darby, D. A., Dyke, A. S., Fitzpatrick, J. J., Funder, S., Holland, M., Jennings, A. E., Miller, G. H., O'Regan, M., Savelle, J., Serreze, M., St.John, K., White, J. W. C. & Wolff, E. 2010. History of sea ice in the Arctic. Quaternary Science Reviews, 29(15), 1757-1778.

Poulain, P. -, Warn-Varnas, A. & Niiler, P. P. 1996. Near-surface circulation of the Nordic Seas as measured by lagrangian drifters. Journal of Geophysical Research: Oceans, 101(C8), 18237-18258.

Prentice, M.L. & Matthews, R.K. 1991. Tertiary ice sheet dynamics: The snow gun hypothesis. Journal of Geophysical Research, 96(B4) 6811-6827.

Falkowski, P. G., Katz, M. E., Knoll, A. H., Quigg, A., Raven, J. A., Schofield, O. & Taylor, F. J. R. 2004. The evolution of modern eukaryotic phytoplankton. Science, 305(5682), 354-360.

R Core Team, 2019. R: A language and environment for statistical computing. R Foundation for Statistical Computing, Vienna, Austria. URL: https://www.r-project.org/

Raymo, M. E. 1994. The initiation of Northern Hemisphere Glaciation. Annual Review of Earth and Planetary Sciences, 22(1), 353-383.

Ren, J., Jiang, H., Seidenkrantz, M. & Kuijpers, A. 2009. A diatom-based reconstruction of Early Holocene hydrographic and climatic change in a southwest Greenland fjord. Marine Micropaleontology, 70(3), 166-176.

Reverdin, G., Niiler, P. P. & Valdimarsson, H. 2003. North Atlantic Ocean surface currents. Journal of Geophysical Research - Oceans, 108(C1), 3002.

Reynaud, T. H., Weaver, A. J. & Greatbatch, R. J. 1995: Summer mean circulation in the northwestern Atlantic Ocean. *Journal of Geophysical Research*, 100, 779-816.

Riaux-Gobin, C. & Stumm, K. 2006. Modern archaeomonadaceae from the land-fast ice off Adélie Land, East Antarctica: A preliminary report. Antarctic Science, 18(1), 51-60.

Rossby, T. 1996. The North Atlantic Current and surrounding waters: At the crossroads. Reviews of Geophysics, 34(4), 463-481.

Rudels, B., Fahrbach, E., Meincke, J., Budeus, G. & Eriksson, P. 2002. The East Greenland Current and its contribution to the Denmark Strait overflow. ICES Journal of Marine Science, 59(6), 1133-1154.

Saloranta, T. M. & Haugan, P. M. 2001. Interannual variability in the hydrography of Atlantic Water northwest of Svalbard. *Journal of Geophysical Research,* 106, 13931-13943.

Saloranta, T. M. & Svendsen, H. 2001. Across the Arctic front west of Spitsbergen: High-resolution CTD sections from 1998-2000. Polar Research, 20(2), 177-184.

Seidenkrantz, M. -., Aagaard-Sørensen, S., Sulsbrück, H., Kuijpers, A., Jensen, K. G. & Kunzendorf, H. 2007. Hydrography and climate of the last 4400 years in a SW Greenland Fjord: Implications for Labrador Sea palaeoceanography. The Holocene, 17(3), 387-401.

Seidenkrantz, M., Roncaglia, L., Fischel, A., Heilmann-Clausen, C., Kuijpers, A. & Moros, M. 2008. Variable North Atlantic climate seesaw patterns documented by a Late Holocene marine record from Disko Bugt, West Greenland. Marine Micropaleontology, 68(1), 66-83.

Serreze, M. C., Maslanik, J. A., Scambos, T. A., Fetterer, F., Stroeve, J., Knowles, K., Fowler, C., Drobot, S., Barry, R.G. & Haran, T. M. 2003. A record minimum Arctic sea ice extent and area in 2002. Geophysical Research Letters, 30(3), 1110.

Schlitzer, R. 2003. eWoce-Electronic Atlas of WOCE Hydrographic and Tracer Data, http://www.ewoce.org/.

Seager, R., Battisti, D. S., Yin, J., Gordon, N., Naik, N. H., Clement, A. C. & Cane, M. A. 2002. Is the Gulf Stream responsible for Europe's mild winters? Quarterly journal of the Royal Meteorological Society, 128, 2563-2586.

Sezerre, M. C., Holland, M. M. & Stroeve, J. 2007. Perspectives on the Arctic's shrinking sea-ice cover. Science, 315(5818), 1533-1536.

Shakun, J. D. & Carlson, A. E. 2010. A global perspective on Last Glacial Maximum to Holocene climate change. Quaternary Science Reviews, 29(15), 1801-1816.

Shakun, J.D., Clark, P. U., He, F., Marcott, S.A., Mix, C., Liu, Z., Otto-Bliesner, B., Schmittner, A. & Bard, E. 2012. Global warming preceded by increasing carbon dioxide concentrations during the Last Deglaciation. Nature, 484(7392), 49-54.

Soltwedel, T., Miljutina, M., Mokievsky, V., Thistle, D. & Vopel, K. 2003. The meiobenthos of the Molloy Deep (5600 m), Fram Strait, Arctic Ocean. Vie et Milieu, 53(1), 1-13.

Stephens, C. J., Antonov, I., Boyer, T. P., Conkright, M. E., Locarnini, R. A., O'Brien, T. D. & Garcia, H. E. 2002. In World Ocean Atlas 2001, Volume 1: Temperature, NOAA Atlas NESDIS, Vol. 49, edited by S. Levitus, 167pp., U.S. Gov. Print. Off., Washington D.C.

Stickley, C. E., Koç, N., Brumsack, H-J., Jordan, R. W. & Suto, I. 2008. A siliceous microfossil view of Middle Eocene Arctic paleoenvironments: A window of biosilica production and preservation. Paleoceanography, 23(1).

Talwani, M. & Eldholm, O. 1977. Evolution of the Norwegian-Greenland Sea. GSA Bulletin, 88(7), 969-999.

Tang, C. C. L., Ross, C. K., Yao, T., Petrie, B., DeTracey, B. M. & Dunlap, E. 2004. The circulation, water masses and sea-ice of Baffin Bay. Progress in Oceanography, 63(4), 183-228.

Tanhua, T., Olsson, K. A. & Jeansson, E. 2005. Formation of Denmark Strait overflow water and its hydro-chemical composition. Journal of Marine Systems, 57(3), 264-288.

Taylor, A. H. & Stephens, J. A. 1998. The North Atlantic Oscillation and the latitude of the Gulf Stream. Tellus A, 50(1), 134-142.

Ter Braak, C. J. F. & Juggins, S. 1993. Weighted averaging partial least squares regression (WA-PLS): An improved method for reconstructing environmental variables from species assemblages. Hydrobiologia, 269-270, 485-502.

Ter Braak, C.J.F. & Šmilauer P. 2012. Canoco reference manual and user's guide: software for ordination, version 5.0. Microcomputer Power, Ithaca, USA, 496pp.

Tréguer, P., Nelson, D. M., Van Bennekom, A. J., DeMaster, D. J., Leynaert, A. & Quéguiner, B. 1995. The silica balance in the world ocean: A reestimate. Science, 268(5209), 375-379.

Tremblay, J. É., Gosselin, M. & Archambault, P. 2014. Marine Biological Hotspots: Ecosystem Services and Susceptibility to Climate Change. Arctic Net Annual Research Compendium (2013-14), 31pp.

Vinje. T. 2001. Fram Strait ice fluxes and atmospheric circulation. Journal of Climate, 14(16), 3508-3517.

Vogt, P. R. 1986. Geophysical and geochemical signatures and plate tectonics. In: The Nordic Seas, edited by Hurdle, B. G. Springer Verlag, New York.

von Quillfeldt, C. H. 1997. Distribution of diatoms in the Northeast Water Polynya, Greenland. Journal of Marine Systems, 10(1), 211-240.

von Quillfeldt, C. H. 2000. Common diatom species in Arctic Spring blooms: Their distribution and abundance. Botanica Marina, 43(6).

von Quillfeldt, C. H. 2001. Identification of some easily confused diatom species in Arctic Spring blooms. Botanica Marina, 44(4). 375-389.

Vorren, T. O., Laberg, J. S., Blaume, F., Dowdeswell, J. A., Kenyon, N. H., Mienert, J., Rumohr, J. & Werner, F. 1998. The Norwegian Greenland Sea continental margins: morphology and Late Quaternary sedimentary processes and environment. Quaternary Scientific Review, 17, 273-302.

Wadhams, P. 2000. Ice in the Ocean. Gordon and Breach Science Publishers, 351pp.

Wang, J. 1993. Interannual variability of sea-ice cover in Hudson Bay, Baffin Bay and the Labrador Sea, and numerical simulation of ocean circulation and sea-ice cover in Hudson Bay. University of Quebec at Chicoutimi, Canada. (PhD Thesis).

Waters, C. N., Zalasiewicz, J., Summerhayes, C., Barnosky, A. D., Poirier, C., Galuszka, A., Cearreta, A., Edgeworth, M., Ellis, E. C., Ellis, M., Jeandel, C., Leinfelder, R., McNeill, J. R. & deB Richter, D. 2016. The Anthropocene is functionally and stratigraphically distinct from the Holocene. *Science, 351*(6269), aad2622.

Weckström, K., Massé, G., Collins, L. G., Hanhijärvi, S., Bouloubassi, I., Sicre, M., Seidenkrantz, M., Schmidt, S., Andersen, T., Andersen, M. L., Hill, B. & Kuijpers, A. 2013. Evaluation of the sea ice proxy IP25 against observational and diatom proxy data in the SW Labrador Sea. Quaternary Science Reviews, 79, 53-62.

Wetterich, S., Viehberg, F. A., Pienitz, R. & Schirrmeister, L. 2008. Ecological training set of freshwater Ostracods in Canadian and Siberian periglacial regions. European Geosciences Union (EGU) General Assembly, 2008.

Williams, K. M. 1986. Recent Arctic marine diatom assemblages from bottom sediments in Baffin Bay and Davis Strait. Marine Micropaleontology, 10(4), 327-341.

Williams, K. M. 1990. Late Quaternary paleoceanography of the western Baffin Bay region: Evidence from fossil diatoms. Canadian Journal of Earth Sciences, 27(11), 1487-1494.

Williams, K. M. 1993. Ice sheet and ocean interactions, margin of the East Greenland Ice Sheet (14 ka to present): Diatom evidence. Paleoceanography, 8(1), 69-83.

Witak, M., Wachnicka, A., Kuijpers, A., Troelstra, S. R., Prins, M. A. & Witkowski, A. 2005. Holocene North Atlantic surface circulation and climatic variability: Evidence from diatom records. The Holocene, 15(1), 85-96.

Witkowski, A., Lange-Bertalot, H. & Metzeltin, D. 2000. Diatom flora of marine coasts. Iconographia Diatomologica, 7, 1-925.

Woodgate, R. A., Fahrbach, E. & Rohardt, G. 1999. Structure and transports of the East Greenland Current at 75°N from moored current meters. Journal of Geophysical Research: Oceans, 104(C8), 18059-18072.

Xiao, X., Zhao, M., Knudsen, K. L., Sha, L., Eiríksson, J., Gudmundsdóttir, E., Jiang, H. & Guo, Z. 2017. Deglacial and Holocene sea–ice variability north of Iceland and response to ocean circulation changes. Earth and Planetary Science Letters, 472, 14-24.

Data

Maps throughout this thesis were created using ArcGIS® software by ESRI. ArcGIS® and ArcMap™ are the intellectual property of ESRI and are herein under licence. Copyright ©ESRI. Map vector and raster data was downloaded from ESRI, Google Earth Pro (SIO, NOAA, U.S. Navy, NGA, GEBCO, IBCAO, USGS) and Natural Earth

Cover Photo:

Valeria Verkhorubova (08/1/13) – Accessed on 01/04/19 from:
https://www.kp.md/daily/26114.4/3008941

9. APPENDICES

Appendix 1: Original counts from the Northern North Atlantic training set

Site	F. arctica	F. oceanica	F. reginae-Jahniae	Archaeomonas sp.	Lat (DMS)	Lon (DMS)	aSST(°C)	aSIC(%)
JM06-WP-19-MC	2	8	1	16	78° 0' 27.936'' N	2° 18' 6.228'' W	2	21.8
JM06-WP-21-MC	1	26	1	14	77° 0'7.34"N	3°14'11.83"W	2.5	15.2
JM06-WP-24-MC	3	6	1	16	74°22'48.00"N	11° 6'43.56"W	1.7	33.9
JM06-WP-26-MC	2	8	4	37	74°32'5.64"N	10°27'39.60"W	2	45.8
JM06-WP-07-BC	1	24	8	11	78°31'34.32"N	7°12'16.52"W	4.1	0
JM06-WP-12-BC	5	31	9	19	78°32'40.60"N	2°14'57.08"E	2.7	10.7
JM06-WP-10-BC	9	45	15	57	78°33'42.34"N	5°14'26.70"E	3.6	0
JM06-WP-16-MC	4	46	18	36	78°32'15.61"N	0°10'8.98"E	2.1	33.8
JM06-WP-14-BC	5	46	18	16	78°33'31.97"N	1° 3'52.56"E	2.4	24.2
JM07-WP-182-MC	4	21	2	93	77°18'19.44"N	0° 1'21.72"W	2.6	1.9
JM07-WP-180-MC	3	7	1	62	77°17'9.96"N	2° 1'31.44"W	2	11.8
JM07-WP-176-MC	12	91	17	38	69°30'57.06"N	22° 4'44.62"W	1.4	80.1
JM07-WP-170-MC	2	8	1	18	73°26'55.43"N	14° 7'10.42"W	1.3	59.5
JM07-WP-171-MC	3	1	0	11	73°27'40.97"N	13° 3'37.08"W	1.6	41.8
JM07-WP-172-MC	3	2	0	11	73°28'14.88"N	12°12'59.04"W	2	35.4
JM08-WP-337-MC	11	30	17	71	78° 4'52.68"N	8°18'14.80"E	4.5	0
JM08-WP-338-MC	5	41	14	23	78° 6'1.04"N	6°19'38.32"E	3.9	0.5
JM08-WP-339-MC	3	5	1	24	77°35'50.32"N	5°35'0.74"E	4.4	0.3
JM08-WP-341-MC	0	14	2	36	77°35'49.92"N	4° 4'27.91"E	4.2	0
JM08-WP-344-MC	5	27	11	57	75°35'21.77"N	8°11'37.82"E	6.4	0
JM08-WP-345-MC	5	38	11	74	75°35'48.55"N	11° 0'3.71"E	6.6	0
JM08-WP-348-MC	7	27	6	34	75°35'50.53"N	13°10'44.11"E	6.3	2.4
JM08-WP-350-MC	4	41	8	16	76°28'43.97"N	14°35'17.12"E	5.4	33
HU2008-029-002	5	44	4	29	61°27'49.25"N	58° 2'9.02"W	6.4	19.5
HU2008-029-006	6	62	28	15	64°23'35.34"N	58° 8'4.96"W	4.6	62.7
HU2008-029-010	3	5	2	24	68°39'59.54"N	59°59'59.82"W	3.3	96
HU2008-029-014	0	3	6	59	70°27'42.52"N	64°39'26.78"W	2.9	97.8
HU2008-029-019	8	24	18	25	75°28'7.39"N	70°38'4.45"W	2.8	94.5
HU2008-029-028	70	44	21	42	76°58'43.89"N	71°53'25.84"W	2.4	80.3
HU2008-029-032	46	57	25	56	76°19'43.62"N	71°25'15.82"W	2.4	84.3
HU2008-029-036	90	77	33	21	76°34'22.81"N	73°57'19.37"W	2.2	82.4
HU2008-029-040	61	42	25	25	75°34'45.79"N	78°37'46.49"W	3.3	78.8

HU2008-029-047	80	49	19	31	74° 1'23.40"N	77° 6'58.79"W	3.4	97.8
HU2008-029-055	91	61	30	26	74° 5'31.43"N	78°43'7.10"W	3.4	95.9
HU2008-029-063	1	1	1	61	72°24'23.00"N	67°43'0.08"W	2.9	99.1
HU2008-029-068	0	37	22	18	68° 13' 41.34'' N	57° 37' 5.016'' W	4	89
KG2	20	61	45	21	65°59'58.20"N	60°29'58.56"W	2.8	86.9
MC688	0	5	0	5	62°32'35.16"N	52°37'55.56"W	5.1	0
MC690	3	2	1	27	68°58'7.21"N	59°34'23.38"W	3.3	94.8
MC691	2	5	2	56	72°30'22.68"N	61°57'20.88"W	3	98.2
MC692	3	5	6	224	71°25'31.80"N	70°26'24.00"W	3.4	99
MC693	46	37	17	97	68°50'17.88"N	66°16'12.00"W	3.1	91.3
MC694	9	10	7	132	68°31'48.00"N	68°19'48.00"W	3.3	0
MC695	3	2	3	18	64°59'59.28"N	59° 0'1.80"W	4.2	80
MC696	3	16	1	11	64° 0'0.00"N	57°59'57.48"W	5.6	48.9
MC697	2	42	3	15	62°33'10.08"N	56°28'4.80"W	6.4	17.6

Appendix 2: Original counts from Core MD99-2322 Kangerlussuaq Trough.

Depth (cm)	Age (CE)	F. arctica	F. oceanica	F. reginae-Jahniae	Archaeomonas sp.
170-171	689.647	6	81	13	24
158-159	873.118	10	80	10	22
152-153	891.261	5	82	13	21
149-150	915.537	5	86	9	21
145-146	933.552	6	81	13	22
142-143	951.847	4	89	7	22
139-140	976.146	2	90	8	29
135-136	994.293	6	88	6	30
132-133	1012.5	7	84	9	25
129-130	1030.58	5	87	8	42
125-126	1054.86	8	84	8	48
122-123	1073.01	8	85	7	41
119-120	1091.25	8	85	7	31
115-116	1115.63	3	88	9	16
112-113	1133.77	1	89	10	11
109-110	1151.92	2	94	4	22
105-106	1170.06	6	87	7	33
102-103	1188.23	14	79	7	18
98-99	1214.87	5	81	14	44
96-97	1228.33	7	89	4	42
93-94	1248.71	10	83	7	49
89-90	1275.43	11	83	6	40

86-87	1295.88	5	85	10	40
83-84	1316.07	6	83	11	55
81-82	1329.39	6	84	10	61
78-79	1349.72	12	78	10	52
74-75	1376.66	9	81	10	50
71-72	1396.74	7	85	8	56
68-69	1417.04	8	51	11	39
64-65	1443.96	11	79	10	43
61-62	1464.3	15	75	10	37
58-59	1484.3	13	53	9	60
56-57	1497.9	9	74	9	58